NASA/TM—2007–215135

Heat Transfer and Pressure Drop in Concentric Annular Flows of Binary Inert Gas Mixtures

R.S. Reid, J.J. Martin, D.J. Yocum, and E.T. Stewart*
Marshall Space Flight Center, Marshall Space Flight Center, Alabama

*Graduate Student Research Program employee in support of Marshall Space Flight Center

November 2007

The NASA STI Program…in Profile

Since its founding, NASA has been dedicated to the advancement of aeronautics and space science. The NASA Scientific and Technical Information (STI) Program Office plays a key part in helping NASA maintain this important role.

The NASA STI program operates under the auspices of the Agency Chief Information Officer. It collects, organizes, provides for archiving, and disseminates NASA's STI. The NASA STI program provides access to the NASA Aeronautics and Space Database and its public interface, the NASA Technical Report Server, thus providing one of the largest collections of aeronautical and space science STI in the world. Results are published in both non-NASA channels and by NASA in the NASA STI Report Series, which includes the following report types:

- TECHNICAL PUBLICATION. Reports of completed research or a major significant phase of research that present the results of NASA programs and include extensive data or theoretical analysis. Includes compilations of significant scientific and technical data and information deemed to be of continuing reference value. NASA's counterpart of peer-reviewed formal professional papers but has less stringent limitations on manuscript length and extent of graphic presentations.

- TECHNICAL MEMORANDUM. Scientific and technical findings that are preliminary or of specialized interest, e.g., quick release reports, working papers, and bibliographies that contain minimal annotation. Does not contain extensive analysis.

- CONTRACTOR REPORT. Scientific and technical findings by NASA-sponsored contractors and grantees.

- CONFERENCE PUBLICATION. Collected papers from scientific and technical conferences, symposia, seminars, or other meetings sponsored or cosponsored by NASA.

- SPECIAL PUBLICATION. Scientific, technical, or historical information from NASA programs, projects, and missions, often concerned with subjects having substantial public interest.

- TECHNICAL TRANSLATION. English-language translations of foreign scientific and technical material pertinent to NASA's mission.

Specialized services also include creating custom thesauri, building customized databases, and organizing and publishing research results.

For more information about the NASA STI program, see the following:

- Access the NASA STI program home page at <http://www.sti.nasa.gov>

- E-mail your question via the Internet to <help@sti.nasa.gov>

- Fax your question to the NASA STI Help Desk at 301–621–0134

- Phone the NASA STI Help Desk at 301–621–0390

- Write to:
  NASA STI Help Desk
  NASA Center for AeroSpace Information
  7115 Standard Drive
  Hanover, MD 21076–1320

NASA/TM—2007–215135

Heat Transfer and Pressure Drop in Concentric Annular Flows of Binary Inert Gas Mixtures

R.S. Reid, J.J. Martin, D.J. Yocum, and E.T. Stewart*
Marshall Space Flight Center, Marshall Space Flight Center, Alabama

*Graduate Student Research Program employee in support of Marshall Space Flight Center

National Aeronautics and
Space Administration

Marshall Space Flight Center • MSFC, Alabama 35812

November 2007

TRADEMARKS

Available from:

NASA Center for AeroSpace Information
7115 Standard Drive
Hanover, MD 21076–1320
301–621–0390

This report is also available in electronic form at
<https://www2.sti.nasa.gov>

TABLE OF CONTENTS

1. GENERAL PROJECT OVERVIEW 1

   1.1 Objective 2
   1.2 Background 2
   1.3 Significance of Results 3

2. LITERATURE REVIEW 4

   2.1 Thermophysical Properties 4
   2.2 Pressure Drop in Annular Channels 7
   2.3 Heat Transfer in Annular Channels 7

3. TEST CONDITIONS 10

   3.1 Test Summary 10
   3.2 Test Matrix 11

4. EXPERIMENTAL APPARATUS 13

   4.1 Gas Circulation Loop Design 14
   4.2 Low-Temperature Loop 14
   4.3 High-Temperature Loop 16
   4.4 Compressor Options 17
   4.5 Test Section Design 18
   4.6 Mechanical Alignment 19
   4.7 Inlet Manifold 20
   4.8 Test Section Inner Tube 20

5. DATA REDUCTION 25

   5.1 Pressure Drop 25
   5.2 Test Section Thermal Equilibrium 26
   5.3 Heat Transfer 27

6. HARDWARE PROCUREMENTS 28

7. STATUS AT CLOSEOUT AND CONCLUSIONS 29

TABLE OF CONTENTS (Continued)

APPENDIX A—THERMOPHYSICAL PROPERTY FITS 30

APPENDIX B—DRAWINGS OF TEST SECTION COMPONENTS 34

APPENDIX C—TEST UNCERTAINTY ANALYSIS 49

C.1 Prandtl Number Uncertainty 49
C.2 Friction Factor Uncertainty for Adiabatic Flows 50
C.3 Nusselt Number Uncertainty 51

REFERENCES 63

LIST OF FIGURES

1. Prandtl number versus mole fraction for three binary gases near room temperature 1

2. Viscosity of He-Ar mixtures from data found in Touloukian[4] (symbols) compared to gas mixture viscosity relation in equation (1) (line). Gas temperature is 291 K 5

3. Thermal conductivity of He-Ar mixtures from accepted values found in Touloukian[3] (symbols) compared to gas mixture thermal conductivity relation in equation (4) (line). Gas temperature is 291 K 6

4. Viscosity of He-Xe mixtures from data found in Touloukian[4] (symbols) compared to gas mixture viscosity relation from equation (1) (line) 6

5. Thermal conductivity of He-Xe mixtures from accepted values found in Touloukian[3] (symbols) compared to gas mixture thermal conductivity relation from equation (4) (line) 6

6. Comparison of Kays correlation (symbols) to Petukhov Popov correlation (solid lines) as a function of Prandtl number and Reynolds number 8

7. Cross-sectional traces of four annular flow passages 10

8. Existing building 4655 test facility 13

9. Single-channel, low-temperature test loop 15

10. Single-channel, high-temperature test loop 16

11. Gas booster pump procured from Haskel for compression of He-Xe mixtures 17

12. Single-channel test section 18

13. Influence of eccentricity and annulus ratio on turbulent-forced convection heat transfer in annular passages 19

14. Honeycomb structure used in manifold near test section entrance 20

15. Temperature of a graphite heater cooled by radiation and conduction alone 22

16. Inner tube assembly: (a) Predrawn and (b) postdrawn 23

LIST OF FIGURES (Continued)

17. Thermal conductivity of Ar gas at low density: accepted values from Touloukian with third-order polynomial fit[3] 30

18. Dynamic viscosity of Ar gas at low density: accepted values from Touloukian with third-order polynomial fit[4] 30

19. Thermal conductivity of He gas at low density: accepted values from Touloukian with third-order polynomial fit[3] 31

20. Dynamic viscosity of He gas at low density: accepted values from Touloukian with third-order polynomial fit[4] 31

21. Thermal conductivity of N_2 gas at low density: accepted values from Touloukian with third-order polynomial fit[3] 32

22. Dynamic viscosity of N_2 gas at low density: accepted values from Touloukian with third-order polynomial fit[4] 32

23. Thermal conductivity of Xe gas at low density: accepted values from Touloukian, Jain, and Jody with third-order polynomial fit[3,28,29] 33

24. Dynamic viscosity of Xe gas at low density: accepted values from Touloukian with third-order polynomial fit[4] 33

25. Deviation in third-order thermal conductivity curve fits from accepted values found in Touloukian and Jody[3,29] 33

26. Deviation in third-order dynamic viscosity curve fits from accepted values found in Touloukian and Jody[4,29] 33

27. Single-channel test section assembly 35

28. Inlet flange manifold 36

29. Inlet flange manifold—pipe with spider attachment 37

30. Centering spider 38

31. Spider attachment 39

32. Inlet centering ring 40

LIST OF FIGURES (Continued)

33. Inlet flange 41

34. Inner tube plug 42

35. Jacket pipe 43

36. Inner tube predraw assembly 44

37. Inner tube postdraw assembly 45

38. Exit manifold 46

39. Outlet centering ring 47

40. Outlet manifold 48

LIST OF TABLES

1. Channel dimensions for single-channel test 10
2. Nominal tests 11
3. Test section power requirements (W) for He-Ar mixtures at $Re = 30{,}000$ 21
4. Hydrodynamic entrance lengths for test sections in turbulent flow 25
5. Jacket time constants 26
6. Flange time constants 26
7. Uncertainties in friction factor measurement for $r^* = 0.76$, He-40%Ar 51
8. Uncertainties in friction factor measurement for He-40%Ar mixtures 51
9. Uncertainty in experimental variables and results at $r^* = 0.833$ 58
10. Uncertainty in experimental variables and results at $r^* = 0.767$ 59
11. Uncertainty in experimental variables and results at $r^* = 0.714$ 60
12. Uncertainty in experimental variables and results at $r^* = 0.500$ 61

LIST OF ACRONYMS AND SYMBOLS

Ar	argon
ASTM	American Society for Testing and Materials
CAD	computer-aided drawing
CFD	computational fluid dynamics
He	helium
ID	inside diameter
MSFC	Marshall Space Flight Center
N_2	nitrogen
OD	outside diameter
TM	Technical Memorandum
Xe	xenon

NOMENCLATURE

A	heat transfer area (m^2)
A_c	cross-sectional area (m^2)
A_{lead}	area across lead (m^2)
A_{tube}	area across tube (m^2)
Bi	Biot number
c	heat capacity
c_g	gas specific heat (J/kg-K)
c_p	specific heat capacity at constant pressure (J/kg-K)
c_s	stainless steel heat capacity (J/kg-K)
c_v	specific heat capacity at constant volume (J/kg-K)
d	thermocouple diameteral location (m); hydraulic diameter
d_{cu}	diameter of copper lead (m)
d_h	hydraulic diameter (m)
D_i	jacket inside diameter (m)
d_i	inner tube inside diameter (m)
D_o	jacket outside diameter (m)
d_o	inner tube outside diameter (m)
dR	distance flange to surface (m)
dr	distance tube to surface (m)
D_s	insulation outside diameter (m)
E	terminal voltage (V)
e	eccentricity
f	friction factor
Fo	Fourier number

NOMENCLATURE (Continued)

h	gas heat transfer coefficient (W/m^2-K)
I	current to test section (A)
K	coefficient
k	conductivity
k_g	gas thermal conductivity (W/m-K)
K_i	inlet coefficient
k_i	insulation thermal conductivity (W/m-K)
k_M	thermal conductivity of gas mixture (W/m-K)
K_o	outlet coefficient
k_s	stainless steel thermal conductivity (W/m-K)
L	length
L_a	test section active length (m)
L_e	entrance length (m)
L_t	test section total length (m)
M	molecular weight
m	mass flow rate (kg/s)
Nu	Nusselt number
n	mole fraction
P	absolute pressure (Pa)
Pr	Prandtl number
Q	internal energy
q	power supplied to inner tube (W)
q'''	volumetric heating rate (W/m^3)
q/A	power supplied per unit area supplied to gas

NOMENCLATURE (Continued)

q_{lead}	total power dissipated by lead (W)
Q_o	initial internal energy (J)
q_o	heat loss (W)
q_t	total power dissipated by inner tube (W)
R	resistance of test section (ohm); inner tube wall thickness (m); thermocouple to adiabatic face distance (m)
r	distance of the thermocouple for adiabatic face
r^*	annulus ratio, d_o/D_i
r_{cu}	resistivity copper leads (ohm-m)
Re	Reynolds number
r_s	stainless steel resistivity (ohm-m)
T_a	room temperature (K)
T_g	bulk gas temperature (K)
T_i	inlet temperature to test section (K)
tir	total indicated runout
T_o	outlet temperature from test section (K)
T_t	temperature of embedded thermocouple (K)
T_w	temperature at inner tube surface (K)
T_∞	temperature of surroundings (K)
V	gas velocity (m/s)
x	measurement position (m)
Δp	pressure drop (Pa)
Δp_a	acceleration pressure drop (Pa)
Δp_f	friction pressure drop (Pa)
Δp_i	inlet pressure drop (Pa)

NOMENCLATURE (Continued)

Δp_o	outlet pressure drop (Pa)
Δp_t	total pressure drop (Pa)
Δx	spacing between pressure taps (m)
ε	surface roughness
ϕ	factor
ϕ_{AB}	factor
γ	ratio of specific heat
μ	viscosity (kg/m-s)
μ_g	gas viscosity (kg/m-s)
ρ	density
ρ_g	gas density (kg/m^3)
ρ_i	inlet gas density (kg/m^3)
ρ_o	outlet gas density (kg/m^3)
ρ_s	stainless steel density (kg/m^3)
τ	time constant (s)
τ_f	time constant for flange (s)
τ_t	time constant for tube (s)
ξ	factor defined by equation (9)
Ψ	factor

TECHNICAL MEMORANDUM

HEAT TRANSFER AND PRESSURE DROP IN CONCENTRIC ANNULAR FLOWS OF BINARY INERT GAS MIXTURES

1. GENERAL PROJECT OVERVIEW

NASA Marshall Space Flight Center (MSFC) builds components for nonnuclear thermal-hydraulic testing of fast spectrum reactor cooling systems for advanced, high-powered, deep-space probes and surface power systems. One option under consideration is to couple a gas-cooled reactor with annular flow passages to closed-loop gas turbine engines. Such engines use mixtures of heavy and light inert gases (typically helium (He)-xenon (Xe)) to reduce core and heat exchanger size and to decrease the number of compression stages.[1] A notable feature of mixtures of gases with differing molecular weight is that they have unusually low Prandtl numbers (*Pr*). Figure 1 compares the Prandtl number of three different gas mixtures as a function of the lighter gas fraction (in all cases, He). This activity focuses on an experimental investigation of Prandtl number effects using test sections with various annulus ratios.

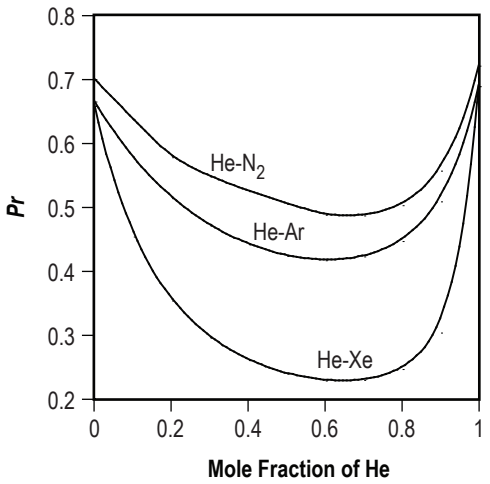

Figure 1. Prandtl number versus mole fraction for three binary gases near room temperature.

1.1 Objective

The principle objective of this test program is to investigate heat transfer coefficients in centrally heated annular ducts at low Prandtl numbers. The immediate need is to obtain data that will be used for comparison to analytical models and existing heat transfer correlations to guide reactor design. Specifically, the data will address two issues previously identified as the low Prandtl number heat transfer effect and the large channel decrement effect. These effects could potentially impact reactor design. Specific supporting objectives are as follows:

- Provide Nusselt number (*Nu*) data using He-argon (Ar) gas mixtures for various annular duct geometries over a range of operating conditions.

- Compare results to existing correlations and recommend correlation for design use.

The completion of this test phase will lead to tests to investigate heat transfer at prototypic temperatures and pressures using He-Xe gas.

1.2 Background

Current reactor design work supporting Project Prometheus is focused on a gas-cooled reactor using an He-Xe coolant mixture. Prototypic thermal hydraulic data are required for ongoing design development. These data include pressure drop and heat transfer characteristics for the geometries and system conditions currently under consideration. In addition, two issues have arisen that are affecting the analytical design of the reactor:

- Lack of heat transfer correlations for gas mixtures with Prandtl numbers of ≈0.2.

- Potential correlation inaccuracy in evaluation of coolant passages with large thickness/diameter.

The range of gas molecular weight under consideration is 20 to 40 g/mole. The baseline He-Xe core inlet temperature is 890 K and the outlet temperature is 1,150 K. The core inlet temperature could vary between 810 and 900 K. The core outlet temperature could vary between 1,050 and 1,150 K. The baseline pressure for the reactor design is 2 MPa, with a range of 1.38 to 2.5 MPa pressure being considered. In support of other activities, MSFC has assembled a single-channel test rig for characterization of pressure drop and heat transfer rates through an electrically heated gas channel.[2] Nitrogen (N_2) flowed through this rig in an open, single-pass arrangement. MSFC has been tasked to modify the single-channel test article for heat transfer and pressure drop characterization of various gas mixtures. Test sections of immediate interest include annular pin, circular ducts, and axial flow open lattice configurations. Test data generated will include pressure drop, and surface and bulk temperatures sufficient to derive the heat transfer coefficient and friction coefficient as a function of system conditions and local position. First priority will be given to the existing annular pin test configuration with a smooth fuel tube insert. All annular tests will have a heated core tube and adiabatic outer tube. Tests may also be conducted on an electrically heated tube to determine correlations for in-tube (nonannular) flow. It follows then that the annulus ratios under consideration may range $0 < r^* < 1$.

1.3 Significance of Results

The film temperature drop is a large contributor to the overall fuel system temperature. Heat transfer test results were intended to guide the reactor methods development in support of gas-cooled reactor design. The results to be obtained have the potential to dramatically change the reactor thermal design (30%–50% heat transfer decrement). Recent computational fluid dynamics (CFD) analyses have indicated that increasing coolant passage thickness can result in a lower heat transfer coefficient than is predicted by correlations. Testing of various sized coolant passages will investigate this analytical trend.

2. LITERATURE REVIEW

2.1 Thermophysical Properties

Problems involving fluid flow and heat transfer of gas mixtures requires knowledge of the viscosities, thermal conductivities, and Prandtl numbers as a function of composition and temperature. Direct measurements of such properties for pure species have been, in most cases, conducted over a wide range of temperature for rarefied gases. Transport properties for pure gases, such as viscosity and thermal conductivity, can be found using polynomial curve fits as a function of temperature. Higher order polynomial curve fits for pure gases have been made from accepted values found in Touloukian.[3,4] These properties are found in appendix A.

The Prandtl number is defined as $Pr = \mu c_p / k$. For a monatomic ideal gas, the gas constant is $R = c_p - c_v$ and the ratio of specific heat, $\gamma = c_p / c_v$, is 5/3, so the specific heat capacity at constant pressure is $c_{p,1} = R/M_1(1-3/5)^{-1}$. For a mixture of ideal monatomic gases, the heat capacity is $c_{p,M} = m_1 c_{p,1} + (1-m_1)c_{p,2}$, where the mass fraction is $m_1 = n_1 M_1 / n_1 M_1 + (1-n_1)M_2$.

Properties for mixtures have been measured near room temperature and, in some cases, at select temperatures, all for rarified gases. Mixture viscosities and conductivities can be calculated from approximations derived from rigorous kinetic theory of gases as applied to a realistic intermolecular force laws.[5] The relative thermal conductivity and viscosity of binary gas mixtures cannot be obtained by simple averaging of pure gas values. More complex methods of calculation of transport properties of binary mixtures of inert gases have been devised. The viscosity of a mixture of gases can be calculated by an approach attributed by various authors to Sutherland and found in Vanco.[6] For a binary mixture, the viscosity equation can be expressed as

$$\mu_M = \mu_1 \left[1 + \phi_{12} \frac{X_2}{X_1} \right]^{-1} + \mu_2 \left[1 + \phi_{21} \frac{X_1}{X_2} \right]^{-1} , \tag{1}$$

where

$$\phi_{12} = \frac{1.065}{2\sqrt{2}} \left[1 + \left(\frac{\mu_1}{\mu_2} \right)^{1/2} \left(\frac{M_2}{M_1} \right)^{1/4} \right]^2 \left(1 + \frac{M_1}{M_2} \right)^{-1/2} \tag{2}$$

and

$$\phi_{21} = \phi_{12} \left(\frac{\mu_2}{\mu_1} \right) \left(\frac{M_1}{M_2} \right) . \tag{3}$$

The pure gas values are taken to be the values determined by the polynomial curve fits outlined in appendix A. The thermal conductivity of a binary mixture of monatomic gases is calculated with a method using a similar Sutherland formulation:

$$k_M = k_1\left[1+\psi_{12}\frac{X_2}{X_1}\right]^{-1} + k_2\left[1+\psi_{21}\frac{X_1}{X_2}\right]^{-1} \quad , \tag{4}$$

where

$$\psi_{AB} = \phi_{AB}\left[1+2.41\frac{\left(M_A-M_B\right)\left(M_A-0.142M_B\right)}{\left(M_A+M_B\right)^2}\right] \tag{5}$$

and

$$\phi_{AB} = \frac{1.065}{2\sqrt{2}}\left[1+\left(\frac{k_A}{k_B}\right)^{0.5}\left(\frac{M_A}{M_B}\right)^{0.25}\right]^2\left(1+\frac{M_A}{M_B}\right)^{-0.5} \quad . \tag{6}$$

Figures 2 and 3 compare the viscosity and thermal conductivity as a function of He mole fraction for an He-Ar mixture at 291.2 K. Such data for He-Xe exists at only a few discrete temperatures. Similar plots for He-Xe mixtures are shown in figures 4 and 5.

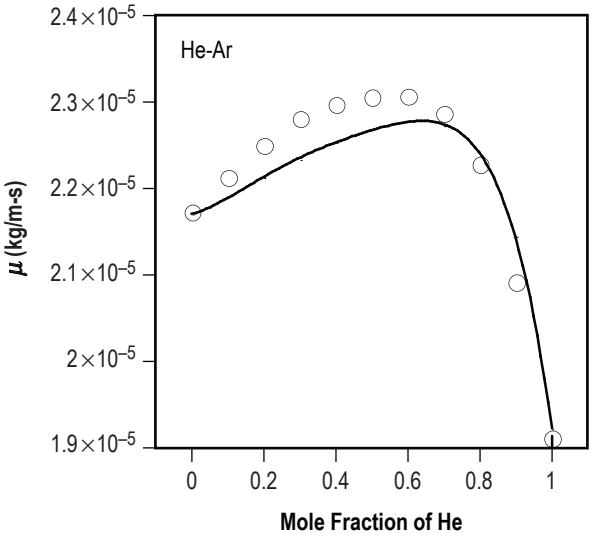

Figure 2. Viscosity of He-Ar mixtures from data found in Touloukian[4] (symbols) compared to gas mixture viscosity relation in equation (1) (line). Gas temperature is 291 K.

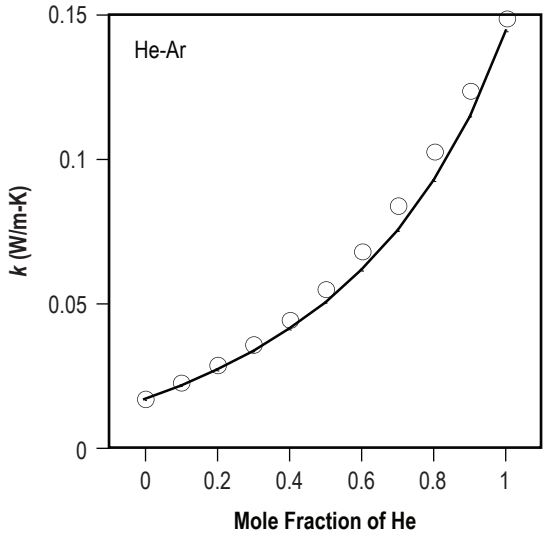

Figure 3. Thermal conductivity of He-Ar mixtures from accepted values found in Touloukian[3] (symbols) compared to gas mixture thermal conductivity relation in equation (4) (line). Gas temperature is 291 K.

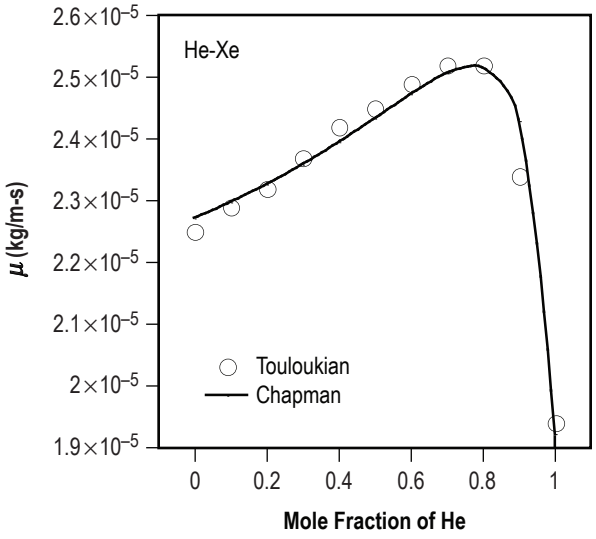

Figure 4. Viscosity of He-Xe mixtures from data found in Touloukian[4] (symbols) compared to gas mixture viscosity relation from equation (1) (line).

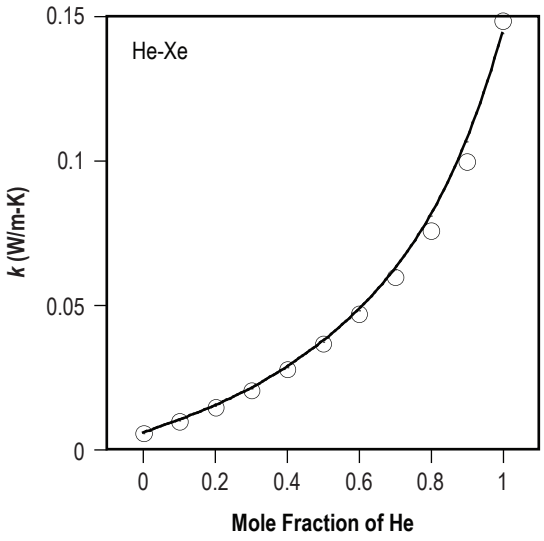

Figure 5. Thermal conductivity of He-Xe mixtures from accepted values found in Touloukian[3] (symbols) compared to gas mixture thermal conductivity relation from equation (4) (line).

2.2 Pressure Drop in Annular Channels

The present study undertakes measurement of friction factors along smooth annular channels as an ancillary to measurement of dimensionless heat transfer. The friction factor, f, for smooth tubes is strictly a function of Reynolds number, $Re = \rho V d_h \mu^{-1}$, where for annular cross sections, the length scale is defined as four times the cross-sectional area occupied by the fluid divided by the wetted perimeter that the fluid exerts skin friction. Fluid friction in annular ducts has been previously characterized in the literature. Walker measured fluid friction factors in smooth concentric annuli in the viscous, transition, and turbulent range.[7] The modified hydraulic radius concept was found adequate to correlate observations. For turbulent flow through a circular tube annuli, Rohsenow recommends use of a Blasius-type friction factor formula: $f = 0.085 Re_{D_e}^{-0.25}$ for $6{,}000 < Re < 300{,}000$.[8]

2.3 Heat Transfer in Annular Channels

Although heat transfer through annular channels has been extensively examined by various groups (for instance, for smooth annuli and for ribbed annuli in He), highly accurate benchmarked heat transfer correlations in the $0.2 < Pr < 0.6$ range have not been systematically developed. Taylor, Bauer, and McEligot document several correlations that could potentially be used in the evaluation of gases with Prandtl numbers of ≈ 0.2.[9] However, few of these correlations were created for use with such gases. In addition, the dimensionless heat transfer coefficients produced by these correlations agree poorly with one another. Testing of the specific geometries under consideration will help guide the designer in the choice of an appropriate correlation.

Investigators that have examined gas flows through channels of similar geometry or Prandtl number condition include Kays and Leung, who considered analytically the heat transfer coefficients of the smooth annulus for a wide range of Reynolds number, annulus ratio, and Prandtl number down to 0.6.[10] Wilson analyzed heat transfer for fully developed turbulent flows in concentric smooth annuli.[11] Taylor, Bauer, and McEligot, and later McEligot and Taylor, considered internal-forced convection in tubes of low Prandtl number gas mixtures.[12,13] They found that two Nusselt relations best captured the Prandtl number dependency for mixtures in the range $0.2 < Pr < 0.7$, the Kays correlation:[14,15]

$$Nu = 0.022\, Re^{0.8}\, Pr^{0.6}\,, \tag{7}$$

and the Petukhov Popov correlation,[16]

$$Nu = \frac{\left(\xi/8\right) RePr}{K_1\left(\xi\right) + K_2\left(Pr\right)\left(\xi/8\right)^{1/2}\left(Pr^{2/3} - 1\right)}\,, \tag{8}$$

where

$$\xi = \left(1.82 \log\left(Re\right) - 1.64\right)^{-2} \tag{9}$$

and

$$K_1\left(\xi\right) = 1 + 3.4\xi \qquad K_2\left(Pr\right) = 11.7 + 1.8 Pr^{-1/3}\,. \tag{10}$$

Figure 6 compares the Kays and Petukhov correlations. Deviation between the two correlations is greatest at low Reynolds number. Other correlations developed for liquid metals or used in heat transfer applications at higher Prandtl number (Colburn and Dittus-Boelter equations[17,18]) were found deficient. Later, the same research group examined turbulent Prandtl number in the near wall region for low Prandtl number flows.[13]

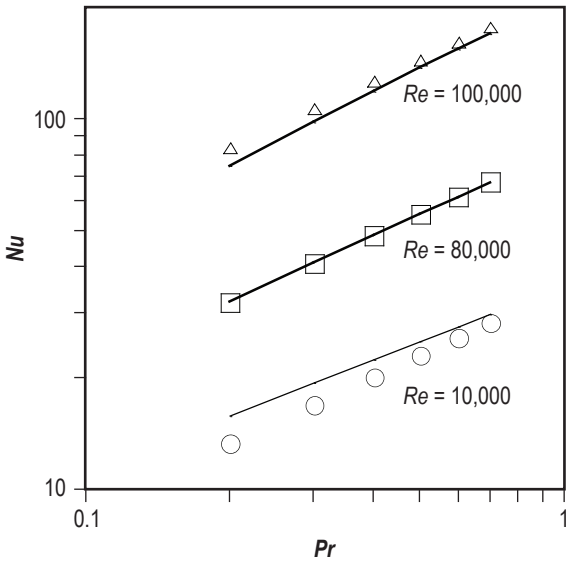

Figure 6. Comparison of Kays correlation[14,15] (symbols) to Petukhov Popov correlation[16] (solid lines) as a function of Prandtl number and Reynolds number.

Heat transfer and pressure drop from augmented surfaces have been also studied. Maubach measured pressure drop through annuli and examined the effect of roughness on turbulent velocity profile of gas-cooled annuli.[19] Dalle-Donne derived correlations for gas-cooled fuel rods with and without rectangular ribs.[20] Ichimiya conducted tests on the effects of several roughness elements on insulated walls for heat transfer from the opposite smooth heated surface in a parallel plate duct.[21] Takase considered turbulent heat transfer performance for He coolant of a fuel rod with spacer ribs for a high-temperature gas reactor.[22]

Of primary importance to this investigation is an understanding of the functional dependences in the Nusselt correlation for fully developed low Prandtl number flows inside annular ducts. For low Prandtl number gas mixtures, the thermal boundary layer develops readily while the momentum boundary layer development lags, provided there exists no unheated starting length. Nusselt correlations typically assume constant thermophysical properties. This assumption may not hold well for the large thermal gradients encountered in the Brayton heat exchangers or reactor core. Accurate gas properties will be needed as a function of temperature and composition. One approach to separate the first-order Nusselt correlation dependencies from fluid property dependencies is to conduct initial tests near ambient temperature where gas mixture properties are well established and constant properties can be assumed. Once a constant property Nusselt relation at low temperature has been established, tests can

be conducted at high temperature and power to separate nonconstant fluid property effects. Later, tests at near prototypic reactor conditions can capture the effects of nondeveloped flow conditions associated with nonuniform axial heating profiles.

3. TEST CONDITIONS

3.1 Test Summary

Table 1 shows nominal dimensions for the channels under evaluation for the single-channel test. Gas in the annulus is heated along the inner tube wall with a uniform heat flux. For the first series of tests, one inner tube size is used and the jacket diameter is changed to produce different annulus ratios. The length of the annulus and heated region of each test section is ≈18 in. The inlet conditions are controlled so that thermal- and hydrodynamic-developed flow exists along a significant fraction of the test section length. The first phase of testing will use an inner tube size of 0.625 in outside diameter (OD). The jacket inside diameter (ID) will be varied (0.750, 0.815, 0.875, and 1.250 in inside diameters) to obtain the different annular ratios. The annular flow channel will be finished to <0.8-μm rms to ensure hydrodyamically smooth surfaces.

Table 1. Channel dimensions for single-channel test.

Test Section Designation	Geometry Type	Inner Tube OD (in)	Jacket ID (in)	Annulus Ratio
AF1	Annulus	0.625	0.750	0.833
AF2	Annulus	0.625	0.815	0.767
AF3	Annulus	0.625	0.875	0.714
AF4	Annulus	0.625	1.250	0.500

Figure 7 shows traces of the four annular duct geometries. Gas in the annulus is heated along the inner tube wall with a uniform heat flux. Care must be taken in the positioning of the inner tube relative to the outer jacket tube to minimize eccentricity of the flow space, as it has been shown by Judd and Wade to have a significant effect on local Nusselt numbers.[8] As will be discussed later, proper positioning is especially important for the test section labeled AF1.

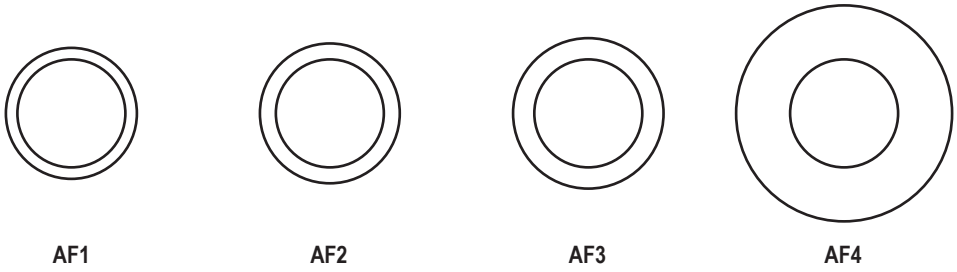

Figure 7. Cross-sectional traces of four annular flow passages.

3.2 Test Matrix

Testing of the single channel will begin with a pure gas, followed by tests with an He-Ar mixture that produces $Pr \approx 0.4$. Initial tests will be near room temperature and focus on heat transfer measurements for constant property flows. Variables in the test conditions include gas composition (Prandtl number) and Reynolds number. Data will be taken near test section thermal equilibrium. Inlet temperature to the single channel will be near room temperature. Table 2 gives the range of conditions for the initial He-Ar test series of each test section.

Table 2. Nominal tests.

Test	Pr	Re
1	0.67	Transition
2	0.67	7,000
3	0.67	15,000
4	0.67	22,000
5	0.67	30,000
6	0.40	Transition
7	0.40	7,000
8	0.40	15,000
9	0.40	22,000
10	0.40	30,000

Variables in the test conditions include He-Ar mixture (Prandtl number) and Reynolds number. Data are to be taken at steady-state conditions for uniform heating of each test section. Inlet temperature to the single channel will be initially near room temperature. Mass flow rate and power is adjusted to create a specified Reynolds number and temperature rise across the test section. For each gas mixture under investigation, the first step will be to identify the transition point from laminar to turbulent flow.

Required data include total power input to test section, mass flow rate, heated surface temperature as a function of axial position, bulk coolant temperature as a function of axial position, pressure at inlet and outlet, incremental pressure drop along the heated region, and calculated Nusselt number for each test condition.

Initial testing will focus on test section AF2 for pure gas testing with Ar followed by He-Ar testing. As a benchmark, pure gas test results will be compared to exiting data in the literature for pure gas heat transfer. After successful acquisition of Prandtl number-sensitivity data with AF2 are complete. He-Ar testing of the remaining test sections will be completed. To ensure data accuracy, repeat data points will be taken for a subset of the test matrix several days or longer after the initial data acquisition. Also, single-sample uncertainty calculations will be made to identify significant error sources. Heat loss testing will be performed to quantify system losses. Zero-power pressure drop testing will be performed. Energy balance calculations for the system will also be performed to verify consistency in the data. Additional data quality information will be produced, including verification of the concentricity of the inner tube and the outer jacket, methodology of ensuring fully developed flow (with supporting evidence), and a procedure for identification of the transition Reynolds number. The expected instrumentation for the first phase of test includes temperature, pressure, pressure drop, gas composition, power to test section, and gas flow rate.

The second phase of this test will require a closed He-Xe loop operated at prototypical conditions—pressure, temperature, flow, and gas composition. Geometry investigations will be focused on the geometry selected at the end of the preconceptual design phase. (Alternate geometries under consideration include circular duct and open lattice flow.)

4. EXPERIMENTAL APPARATUS

The single-channel tests make use of facilities developed for a heat pipe heat exchanger component test.[2] A number of modifications will be made to these facilities to better meet the expanded scope of this test. Figure 8 is a photograph of the existing test facility housed in building 4655 at MSFC. To accomplish the outline testing, a portion of the floor space within the building 4655 high bay was designated to house the setup and operation. An area at the rear of the laboratory with an approximate rectangular footprint of 15×25 ft was set aside. Geometric constraints were defined for each of the primary test support system so a revised laboratory layout could be generated. These systems include the following:

- Test section.
- Test loop.
- Inert gas source.
- House cooling water loop.
- Power distribution system.
- Instrumentation and control.

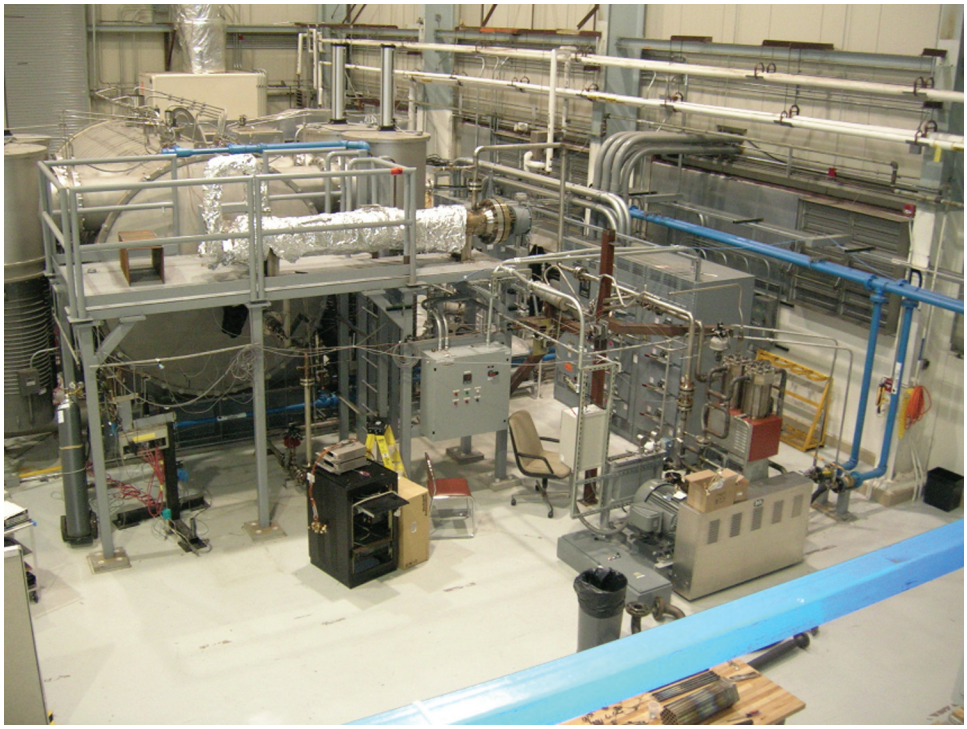

Figure 8. Existing building 4655 test facility.

The location of building 4655 provides close access to both facility water and power interfaces while minimizing interference with normal day-to-day operation. The original facility was configured for single-channel tests with pure N_2 in a single-pass flow arrangement. While an open flow arrangement is appropriate where the gas supply is plentiful, a closed loop better conserves more expensive gases such as Ar or Xe.

Figure 8 is a photograph of the floor space in the summer of 2005 just before hardware setup began. The existing single-channel rig and the racks to house the data acquisition/control hardware and computers are shown on the lower left side.

4.1 Gas Circulation Loop Design

Gas is supplied to the annular test section from a closed circulation loop. The loop and test section as now configured can handle inexpensive gases such as He, Ar, or N_2. Use of more expensive gases like Xe will require a leak-free compressor and a cold trap or other method to recover gas from the loop. Most of the components for a loop testing low-temperature gas can also be used for tests at high temperature. The high-temperature design requires components to preheat and cool the gas on either end of the test section.

4.2 Low-Temperature Loop

Figure 9 shows a schematic of a flow loop for tests near room temperature. The flow loop consists of a main loop and a nested bypass loop. The low-temperature loop is built from austenitic stainless steel and makes use of Conflat flanges or welded joints, whichever is convenient. For the initial series of tests with a reciprocating compressor, the flow in the bypass loop may be as much as 10 times that in the main loop. The test section can be evacuated with a roughing pump located at the exit of the compressor. Gas is supplied to the loop from premixed bottles with composition known to be better than a percent. A residual gas analyzer is used to confirm composition of the circulating gas. Loop pressure is controlled with a Tescom proportional pressure controller that will set the system to a nominal 100 psia. An in-line pressure relief value is connected near the gas supply and compressor exit.

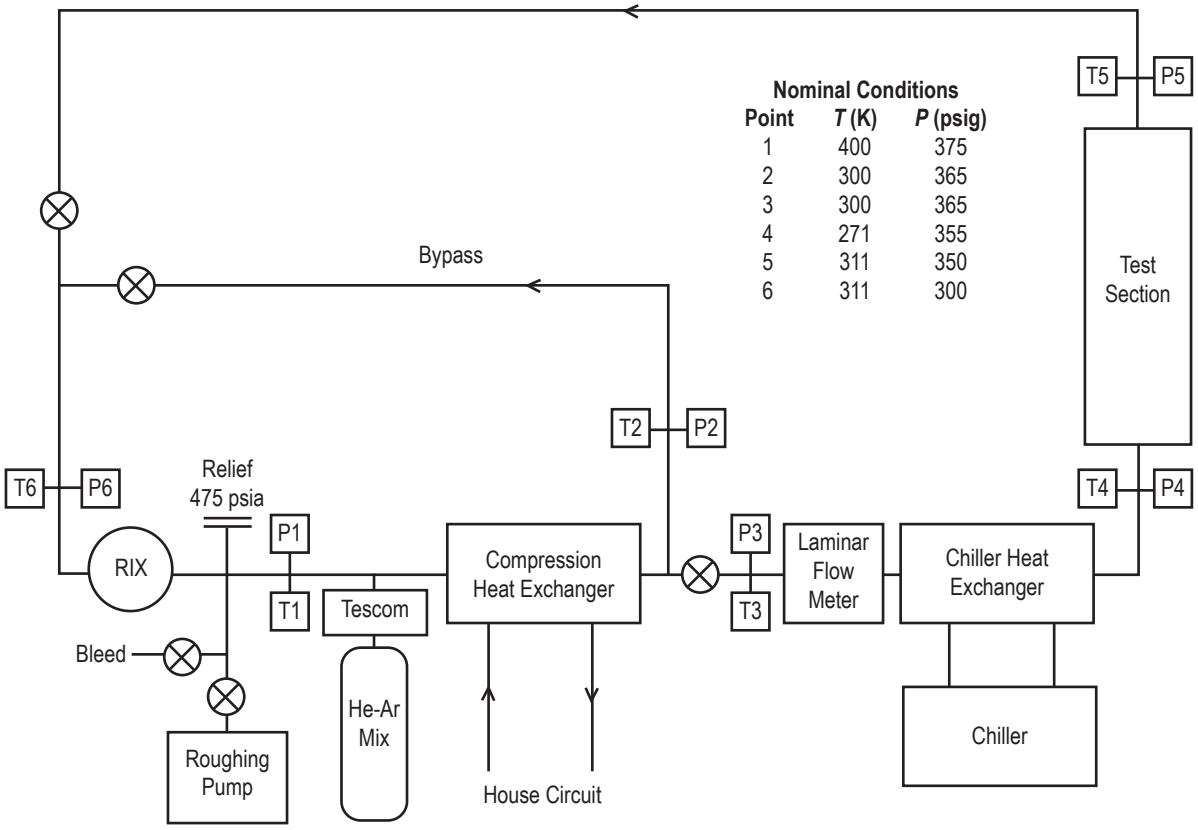

Figure 9. Single-channel, low-temperature test loop.

On exiting the compressor, compression heat is removed from the gas with a heat exchanger connected to a house water circuit. This heat exchanger cools the gas to near room temperature. The flow is then split between the main loop and the bypass loop. The proportion of gas to each loop is established with a variable position valve located in the main line that acts as a throttle and as another valve in the bypass line. Gas enters the main loop. In the previous open-loop system, mass flow rates were measured with a thermal meter that operates with a calibration that has a complex dependence on gas composition and local heat transfer rates. Such a meter would be difficult to use for gas with variable composition.

For the current setup, gas passes through a Meriam Instruments model 50MH10-2 laminar flow element that measures volumetric flow rate. Calibration for the laminar flow meter merely requires knowledge of gas density. The gas may optionally enter a PolyScience model 6706P chiller capable of bringing the gas to ≈263 K. The gas then moves through the test section where it is heated along the annular channel with power supplied from two high direct-current bus bars.

For the initial test series, the temperature rise across the test section will be held constant by controlling the power to the test section at a given mass flow rate. Gas inlet and exit temperatures are measured as well as wall temperature along the inner flow channel and pressure along the outer surface of the channel. Heat loss to the environment is controlled with insulation. Gas exits the test section and passes through a variable position valve before returning to the bypass loop where it is compressed.

Given a suitable compressor or blower, the low-temperature loop can use either He-Ar or He-Xe mixtures. The loop lines were sized with 2-in pipe so as not to exclude the possibility of compressing the gas with a turbo blower. One drawback of larger lines is the added volume of gas required to charge the system. This problem is especially acute for costly Xe. To partly compensate for this, line lengths will be kept short throughout and operating pressure kept to the lowest possible level consistent with compressor design specifications.

4.3 High-Temperature Loop

Figure 10 shows one possible embodiment of a high-temperature gas circulation loop. The bypass portion of the circuit is identical to the low-temperature version. However, the main loop has a number of changes from the low-temperature design, including movement of the laminar flow meter from the test section inlet to downstream of the test section aftercooler. For parts seeing high temperature, metal sealed flanges are impractical, so all welded construction will be mandatory in the main loop near the test section. Also, use of superalloy material may be required if the test section must operate much above 700 °C. On exiting the bypass, the gas enters a preheater that brings the gas to the test section inlet temperature. The gas then enters the test section where it is electrically heated in the annulus. A spider and outlet centering ring, made of alumina, electrically isolate the inner tube from the jacket. Heat loss to the environment is controlled with insulation and electrically heated guard heaters distributed axially along the test section. The gas exits the test section where it is cooled to near room temperature with a heat exchanger (aftercooler) connected to a house circuit. Once cooled, the gas can pass through lines with conventional construction taken from the low-temperature loop.

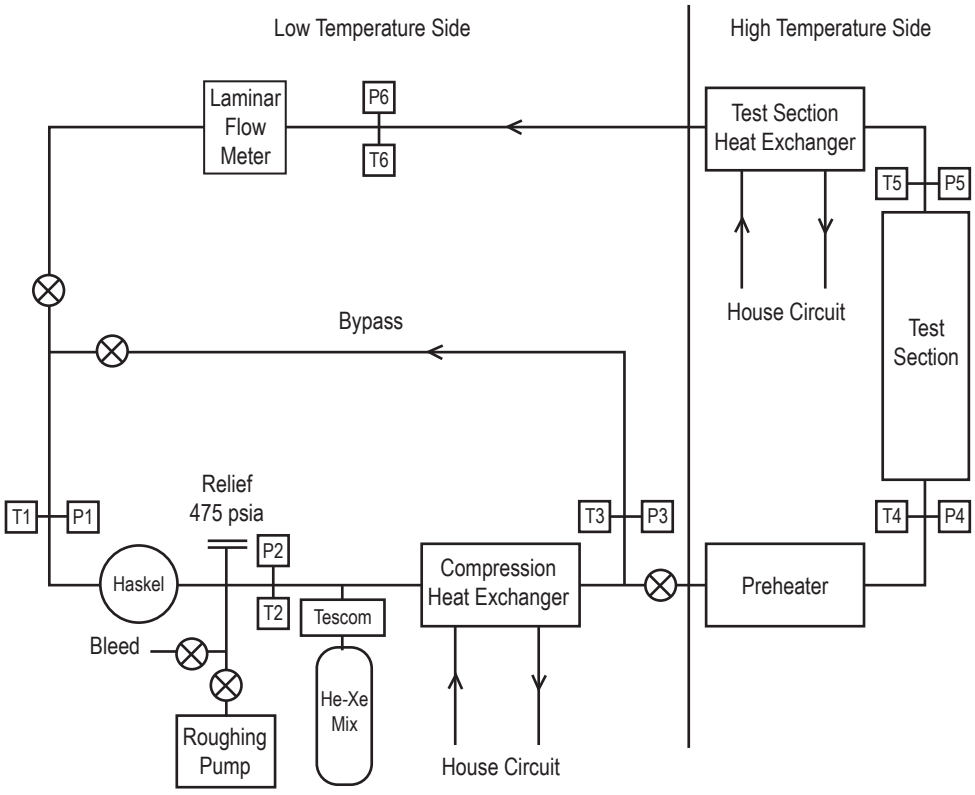

Figure 10. Single-channel, high-temperature test loop.

4.4 Compressor Options

Gas circulation through the loop may be achieved in a number of ways, depending mostly on factors unrelated to operating efficiency. Ideally, the compressor would be capable of handling gases ranging from pure He to pure Xe at high pressure. An industrial, oil-free, high-pressure gas compressor manufactured by RIX Industries, Benicia, CA, is available as part of the existing test facility. This large compressor is capable of circulating up to 0.1 kg/s of pure He from 300 to 375 psia. Such capacity far exceeds what is required for the single-channel test apparatus. However, the gas leakage rate through the RIX compressor's labyrinth seals is quite large, requiring the change of several K bottles of gas during an 8-hr operating period at 100 psia. Use of a compressor that leaks at this rate is an entirely practical option for premixed He-Ar that costs ≈$200 per K bottle. Premixed K bottles of Xe cost over $20,000 each, making the RIX compressor a prohibitively expensive option for an He-Xe system. The RIX compressor will be used for the initial tests with He-Ar. Another leak-tight option must be devised for the He-Xe test series. Candidate compression systems for use with He-Xe include (1) a Metal Bellows model MB-601 pump contained inside a pressurized vessel, (2) a Haskel gas booster pump (fig. 11), and (3) a Fuji ring compressor contained inside a pressurized vessel.

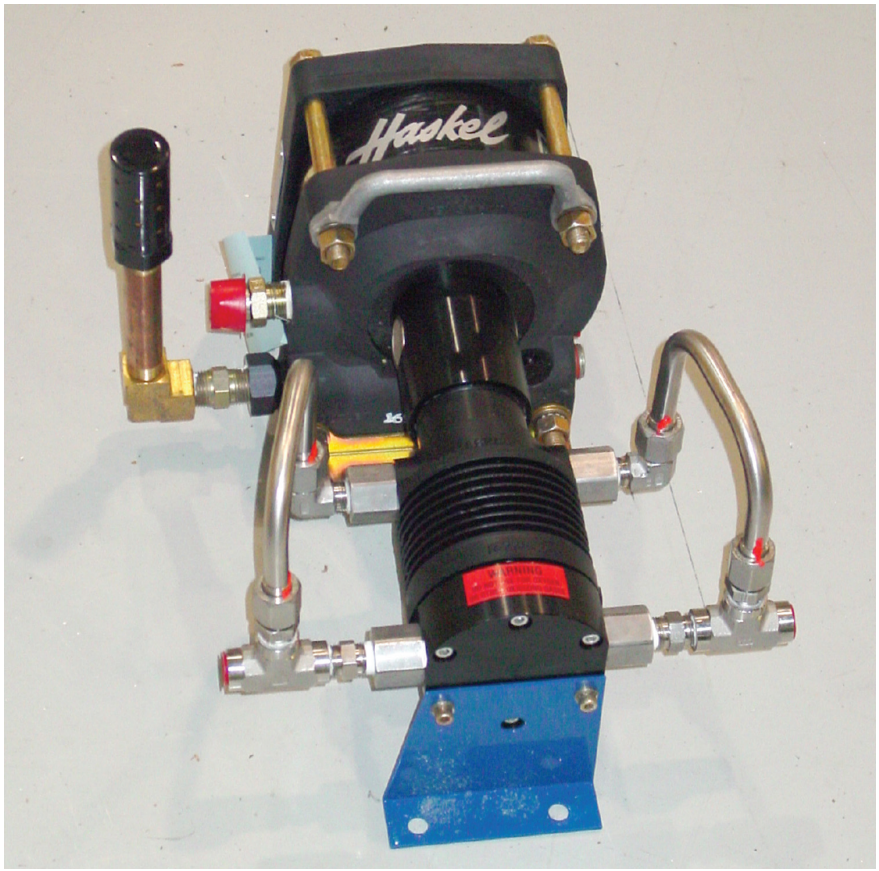

Figure 11. Gas booster pump procured from Haskel for compression of He-Xe mixtures.

4.5 Test Section Design

A CAD rendering of the single-channel test section is shown in figure 12. More detailed drawings of the test section are shown in appendix B. The test section consists of an inlet and exit manifold, jacket tube, and inner tube with associated power feeds, and temperature and pressure sensors. The test section is easy to insulate and permits the inclusion of guard heaters to reduce radial thermal gradients for a high-temperature design. The low-temperature design can be transformed to a high-temperature unit by replacing flanges with welds. Only minor modifications to the test section design are required to change the jacket dimensions for tests at different annulus ratios. The modular design of the test section allows multiple vendors to fabricate subcomponents. The test section may be oriented vertically or horizontally, permitting the effect of natural convection to be examined. By directly heating the jacket tube, and by incorporating an appropriate electrical grounding scheme, this design may be modified for circular tube geometry.

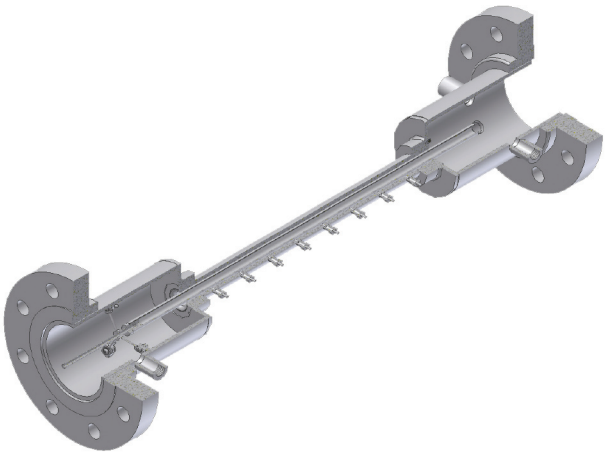

Figure 12. Single-channel test section.

In its present embodiment, the test section is instrumented with 10 embedded 0.01-in-diameter type K sheathed thermocouples with special limits of error with accuracy on the order of $\pm$1.1 °C. These thermocouples are electrically insulated from the sheath to avoid ground loops between the data and power systems. The sheath of each thermocouple is also insulated with polyolefin shrink tube in places where the thermocouple might make contact with the jacket or manifold. Additional sheathed and insulated thermocouples are placed at three locations at both the inlet and exit of the test section to measure the inlet and exit gas temperature.

Pressure taps are placed at eight locations along the test section as well as at the test section entrance and exit. Differential pressure measurements are made along the length of the test section with a multichannel pressure scanner. Manufactured by Pressure Systems, the NetScanner™ model 9116 consists of up to 16 silicon piezoresistive pressure sensors, all referenced to a common port with $\pm$0.05% full-scale accuracy. For this test, model 9116 is instrumented with 7-kPa, full-scale pressure transducers and is capable of operating at line pressures up to 4 MPa. Eight pressure taps are located along the length of the flow annulus with the fourth tap from the test section entrance serving as the reference port.

4.6 Mechanical Alignment

For well-controlled heat transfer measurements, the eccentricity of the inner tube with respect to the jacket tube is a key variable to control, especially when the annulus ratio exceeds ≈0.8. Annulus eccentricity is the distance between the centerlines of the inner and jacket tubes divided by the mean gap between the tubes. Eccentricity can affect local Nusselt numbers as shown in Judd and Wade.[8] Eccentricity is estimated based on measurements of total indicated runout of the inner and jacket tubes for the AF2 test section, which are 0.0085 and 0.005 in, respectively. Using this estimate, the eccentricity of the assembly for test section AF2 is approximately

$$\delta e = \frac{2e^*}{D_i - d_o} \approx \frac{2\left(\left(tir_i\right)^2 + \left(tir_o\right)^2\right)^{1/2}}{D_i - d_o} = \frac{2\left(\left(0.0085\right)^2 + \left(0.005\right)^2\right)^{1/2}}{0.815 - 0.625} \tag{11}$$

$$e = 0 \pm 0.104 \text{ (20 to 1).} \tag{12}$$

Figure 13 shows the relation between eccentricity and local Nusselt number at various annulus ratios. For annulus ratios <0.8 and eccentricity <0.1, an approximate linear relation between Nusselt number and eccentricity can be used: $Nu/Nu_{\text{conc}} \approx 1 - e/2$. Outside these ranges, the relation becomes nonlinear and an evaluation must be made for each annulus ratio. For an annulus ratio of 0.83, the polynomial fit for the eccentricity factor is $Nu/Nu_{\text{conc}} \approx -100\,e^3 + 5\,e^2 - e + 1$.

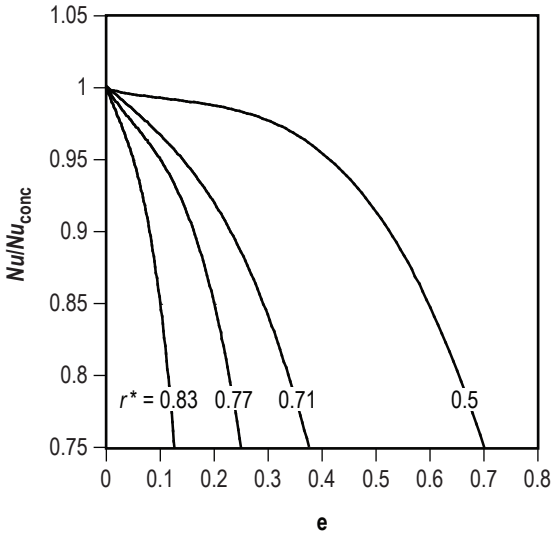

Figure 13. Influence of eccentricity and annulus ratio on turbulent-forced convection heat transfer in annular passages.

Centering rings produce concentric alignment between the inner tube and the jacket. A spider located at the inlet of the test section maintains alignment once the centering ring at the test section inlet is removed. The outlet centering ring is retained after test section assembly, holding the inner tube at the

exit of the annular region. Both the spider and the outlet centering ring are made from G-10 fiberglass (for low-temperature design) or alumina (for high-temperature design) to isolate the electrically heated inner tube from the jacket body. These centering features collectively permit quick changeout and positioning of the inner tube.

4.7 Inlet Manifold

A honeycomb core manufactured by Benecor, Inc., Wichita, KS, is located inside the inlet manifold. This core, shown in figure 14, is a right circular cylinder (4 in diameter by 4 in long) made up of a 0.002-in-thick sheet that forms cells 0.1 in on a side. A hole is cut into the center axis of this core to pass a power lead between the inlet manifold and the inner tube power terminal. This core reduces the Reynolds number of the gas passing through it, providing a definable boundary condition near the inlet of the annular region. The gas then enters a short open region, and then passes into the annular test section through a rounded entrance region with a 0.2-in radius.

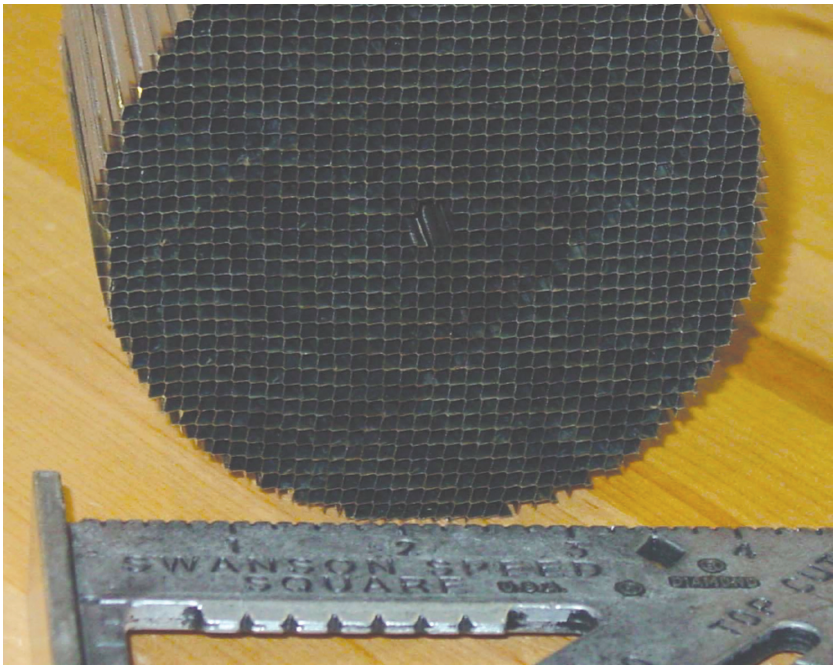

Figure 14. Honeycomb structure used in manifold near test section entrance.

4.8 Test Section Inner Tube

The test section inner tube forms the core of the annulus; as such, it must simulate the dissipation of fission heat. To produce usable heat transfer correlations for fully developed flow conditions, the local heating rate should occur at a known and preferably spatially uniform rate. Table 3 gives the test section power requirement for various gases and annulus ratios to maintain $Re = 30{,}000$ with a 271 K inlet temperature and a 311 K exit temperature. Use of gas mixtures between He-40Ar and He-100Ar span $0.4 < Pr < 0.7$. This covers the same Prandtl number range as He-0Ar to He-39Ar, and owing to the lower heat capacity of Ar, requires less power to heat the test section than with He-rich mixtures.

Table 3. Test section power requirements (W) for He-Ar mixtures at $Re = 30{,}000$.

Test Section	Jacket ID (in)	He-0%Ar	He-40%Ar	He-100%Ar
AF1	0.750	3,283	848	371
AF2	0.815	3,438	888	389
AF3	0.875	3,582	925	405
AF4	1.250	4,477	1,156	506

Two approaches to heating the test section inner tube were considered. One approach uses a graphite resistance heater, recently developed at MSFC for other thermal simulator work. A version of these graphite heaters has a circular cross section with a diameter of 0.3 in, split along the axis, forming two semicircular halves along the heated length. These semicircular halves form a 'U' shape, with the bottom of the 'U' a transition to a circular (nonsplit) cross section at the unheated end opposite the leads. Each graphite semicircular half is separated by electrically insulating spacers. The heater ends at the top of the 'U' connect to power leads. Alumina rings isolate the graphite conductors from the walls of the inner tube assembly. In the current embodiment, this heater is inserted into an annular inner tube having a 0.625-in OD and a 0.457-in ID. Direct current, applied across the leads located at the test section exit, dissipates heat volumetrically.

Use of graphite heaters for this particular application has a serious drawback. Heat transfer between the graphite heater and the inner tube is by radiation, and, in the presence of gas, natural convection. Proper operation of the test article requires heat to be uniformly distributed on the surface of the inner tube. Heat transfer by conduction and radiation are consistent with this requirement. However, natural convection of gas between the hot graphite heater and the cooler inner tube potentially induces nonuniform distribution of heat on the surface of the inner tube and can have strong dependence on the orientation of the test section. Convection can be suppressed by evacuating the volume between the heater and the inner tube. Evacuating the inner tube volume leaves only radiation and conduction to remove heat from the leads. Unfortunately, as shown in figure 15, the leads under these conditions become quite hot, approaching 1,000 K, thus requiring a robust electrically insulating, high-temperature hermetic seal.

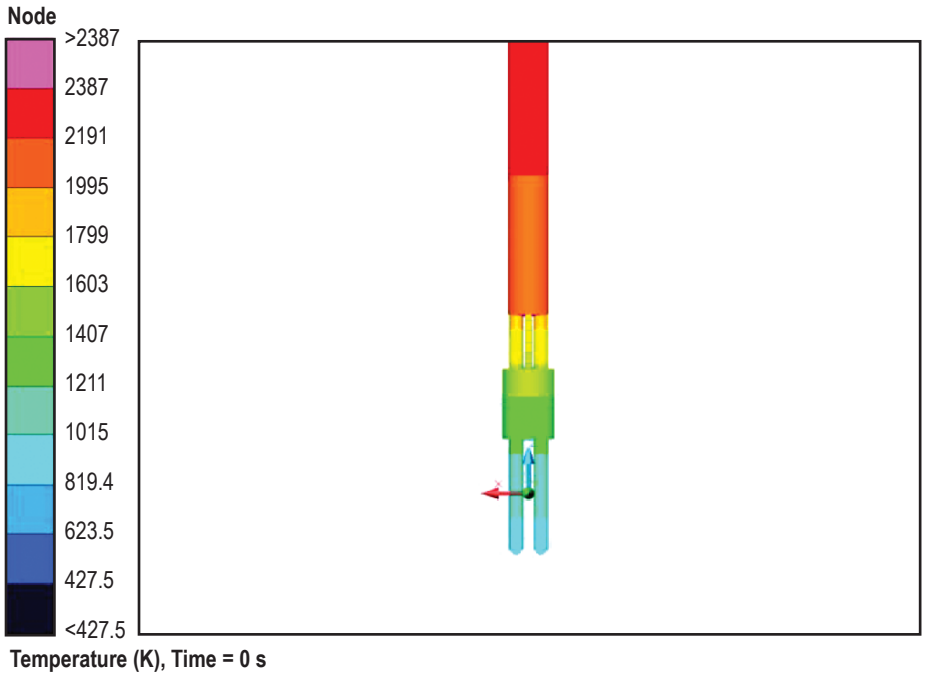

Figure 15. Temperature of a graphite heater cooled by radiation and conduction alone.

To avoid the vexations associated with high-temperature seals, direct resistance heating of the inner tube is now being pursued. In anticipation of this contingency, a 1,400-A, 15-kW power supply was purchased from Lambda Americas, Neptune, NJ. Copper bussing attached to each end of the inner tube that runs to power terminals are located on opposing manifolds. The sheaths of thermocouples that run between the inner tube and the manifolds are electrically isolated from the manifold with polyolefin shrink tube. The heating rate is then established, assuming electrical power is uniformly dissipated to the inner tube with homogeneous composition and cross section. Additional heating or cooling can occur from parasitic losses across insulation that couples the test section gas and the environment:

$$q = EI - \frac{2\pi k_g L\left(T_g - T_\infty\right)}{\ln\left(D_s / D_o\right)} . \tag{13}$$

An ≈2.3-in-thick layer of insulation, having 0.068-W/m-K thermal conductivity, placed on a 1-in-diameter jacket tube is sufficient to keep the second parasitic term <4 W (without other loses).

Figure 16 shows a method of producing axial holes along the 25-in length of the inner tube. These holes can be used to embed temperature probes in the wall of the inner test section tube. Five slots 0.015×0.015 in are cut or milled on the outside diameter of a 0.625-in OD×0.035-in wall tube. A mandrel is slid inside a large bore sheath tube with a 0.75-in OD and 0.02-in wall. This assembly is drawn until the outer tube touches the inner tube. The assembly is then drawn again to the desired OD of the sheath tube. The outer surface can then be machined or otherwise finished.

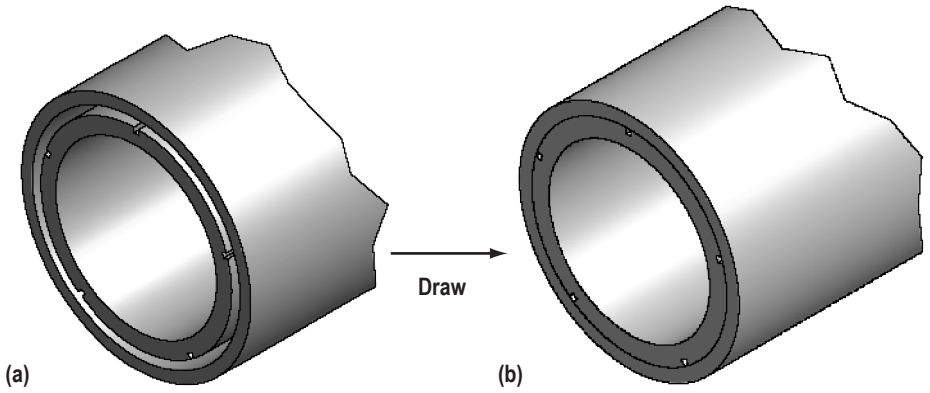

Figure 16. Inner tube assembly: (a) Predrawn and (b) postdrawn.

Test section wall temperatures can be measured by inserting sensors into the axial holes of the inner tube. Two sensor types are possible. Ungrounded type K thermocouples with special error limits having 0.01-in OD sheaths, with a single bead each, allow for up to 10 wall temperature measurements to be made if thermocouples are fed from both ends of the inner tube. Fiber optic temperature sensors, 0.005-in diameter, contained inside a 0.01-in-diameter stainless steel capillary tube can also be used. These sensors, marketed by Luna Innovations, exploit Fabry-Perot interferometry to measure temperature to within ±0.5 °C up to 1,200 °C. Temperature is measured at gratings spaced along the fiber at 1-cm intervals, enabling a single fiber, fed from one end of the inner tube, to make measurements at up to 50 locations. If fiber optic sensors are placed in all five axial holes of the inner tube, up to 250 temperature measurements are possible. Use of thermocouples or fibers in an electrically heated tube requires isolation of the metallic sheath from the grounded jacket and manifold.

Surface temperatures must be inferred from the temperature sensor embedded in the wall of the electrically heated inner tube. To get an accurate reading, the measurement must be corrected for the temperature drop between the thermocouple and the surface. Assume the region around the temperature sensor and the cooled surface can be approximated as a plane wall with uniform energy generation per unit volume, adiabatic on one face and convectively cooled on another. The surface temperature is related to the wall temperature by

$$T_w = T_t - \frac{q''' R^2}{2k_s}\left(1 - \frac{r^2}{R^2}\right),\ 0 \le r \le R\ , \tag{14}$$

where the inner tube wall thickness is R and the distance of the thermocouple from the adiabatic face is r. Given the proposed test conditions, it is anticipated that this correction will be ≈2 °C, for an overall temperature difference between the surface and the gas of 30 °C.

For a constant surface heat flux condition, mean gas temperature as it flows through a channel is a linear function of position:

$$T_g(x) = T_i + \frac{q\pi d_o}{mc_g}x\ . \tag{15}$$

If the outlet temperature and channel length are known, the relation between temperature and position can be simplified to

$$T_g(x) = T_i + (T_o - T_i)\frac{x}{L},\ 0 \le x \le L\ . \tag{16}$$

Provided power is uniformly distributed in the wall, this method of gas temperature calculation should prove satisfactory, with no disturbances to the flow field or ambiguity in the measurement of stream temperature. A contingency, should this approach not work, is to place thermocouples into the pressure taps so that they are flush mounted and out of thermal contact with the jacket.

5. DATA REDUCTION

5.1 Pressure Drop

The annuli tested in this study will have a finish better than 1 μm, yielding $\varepsilon/d = 1\times10^{-4}$, which is effectively smooth at $Re = 30{,}000$. For laminar flow, the entrance region is taken to be $L_e/d \approx 0.06\,Re$. The maximum laminar entrance length, at a Reynolds number of 2,300, is 138 diameters, the longest length possible regardless of regime. For fully turbulent flow, the hydrodynamic entrance region is $L_e/d \approx 4.4\,Re^{1/6}$. Table 4 compares the entrance length to hydraulic diameter ratios for the four annular test sections in the 4,000 to 100,000 Reynolds number range using data recommended for annular flow by Jonsson and Sparrow.[23]

Table 4. Hydrodynamic entrance lengths for test sections in turbulent flow.

L/d_h Re	144 AF1	95 AF2	72 AF3	29 AF4
4,000	22	19	18	15
10,000	25	22	21	18
30,000	30	27	25	21
100,000	37	33	31	26

Pressure measurements will be made at 2-in intervals along the 18-in length of the test section. In the laminar regime, flow will be developing through the entire length of the test section and a fully developed friction factor will not be reached. Above the transition point when $Re > 2{,}300$, with hydraulic diameter <0.25 in, fully developed flow exists along a significant fraction of the test section length. The test section with the largest hydraulic diameter, AF4, has fully developed flow over less than half its length. It is expected that pressure drop across the annular test section will be fully accountable by hydraulic radius correlation once gas viscosity and Reynolds number at composition is properly established.

Kays uses a relation for the friction factor along the fully developed length of a heated annular channel.[24] This relation accounts for friction- and temperature-related acceleration effects:

$$\Delta p = \frac{m^2}{2\rho_i A^2}\left[2\left(\frac{\rho_i}{\rho_o}-1\right)+4f\frac{L}{d_h}\frac{2\rho_i}{\rho_i+\rho_o}\right]. \tag{17}$$

For flows with measurable heat transfer, the mass flow rate can be inferred from the electrical measurements and temperature rise across the test section or the volumetric flow meter. For adiabatic flows, mass flow rate can only be established with the flow meter. Estimates of uncertainty intervals for gas friction factor can be found in appendix C.

5.2 Test Section Thermal Equilibrium

Thermal equilibrium in the test article occurs when thermal gradients across the test section no longer have a time-varying component. A one-dimensional transient conduction analysis for the jacket tube and end flange provides an order of magnitude estimate of the time required for the test section to reach equilibrium after a step change in boundary condition. The Biot number, $Bi = hLk^{-1}$, for the jacket tube was calculated. Here, the jacket wall thickness is used for the length scale, L, in the Biot number of the jacket. The radial distance between the ID of the jacket tube and the OD of the flange is the length scale of the end flanges. Heisler charts[25] were used to find the internal energy change as a function of time for a plane wall of thickness $2L$. This yields the Fourier number corresponding to an internal energy change of $Q/Q_o = 0.99$. The time constant for this change was then calculated using $\tau = \rho_s c_s k_s^{-1} R^2 Fo$. Table 5 shows the results for the jacket including Biot numbers, Fourier numbers, conduction distances, and resulting time constants for the annulus ratios under consideration.

Table 5. Jacket time constants.

Variable	AF1	AF2	AF3	AF4	Units	Description
ρ_s	7,900	7,900	7,900	7,900	kg-m^{-3}	Density of stainless steel
c_s	400	400	400	400	J/kg-K	Heat capacity of stainless steel
k_s	17	17	17	17	W/m-K	Thermal conductivity of stainless steel
h	1,245	819	623	249	W/m-K	Gas heat transfer coefficient
dr	0.25	0.25	0.25	0.25	in	Jacket wall thickness
Bi	0.465	0.306	0.233	0.93	–	Biot number for jacket
Fo	18.5	22.4	26.4	30.3	–	Fourier number for jacket
τ	139	168	208	779	s	Time constant for jacket

Table 6 shows similar results for the flange. The time constant for the flange is about an order of magnitude higher than for the jacket. This reflects the larger volume of the flange relative to the surface area available for heat removal. The jacket tube time constant more accurately describes steady state for the test section. Use of the longer duration flange time constant may be considered a sufficient condition for thermal equilibrium.

Table 6. Flange time constants.

Variable	AF1	AF2	AF3	AF4	Units	Description
ρ_s	7,900	7,900	7,900	7,900	kg-m^{-3}	Density of stainless steel
c_s	400	400	400	400	J/kg-K	Heat capacity of stainless steel
k_s	17	17	17	17	W/m-K	Thermal conductivity of stainless steel
h	1,245	819	623	249	W/m-K	Gas heat transfer coefficient
dR	1.625	1.593	1.563	1.375	in	Radial distance jacket OD to flange
Bi	3.024	1.949	1.454	0.512	–	Biot number for flange
Fo	4.4	7.6	9	15.3	–	Fourier number for flange
τ	1,386	2,321	2,632	3,464	s	Time constant for flange

5.3 Heat Transfer

The test section is assumed sufficiently insulated to keep heat loss a small fraction of the applied power. An electrically heated tube provides power to the test section for the single-channel heat transfer test. This power is determined using measurement of voltage across the test section terminals and the voltage across a known resistance in the circuit. Using heating rate established in equation (13), the correction for temperature drop across the tube wall in equation (14), and the computed gas temperature in equation (15), the Nusselt number is

$$Nu = \frac{qd_h}{A\left(T_w - T_g\right)k_g} \quad , \tag{18}$$

where k_g is the thermal conductivity of the gas, d_h is the hydraulic diameter of the test section channel, q/A is the power supplied per unit area supplied to the gas locally, T_w is the measured wall temperature, and T_g is the gas bulk temperature. Gas thermal conductivity is assessed based on methods outlined earlier in this Technical Memorandum (TM) at the bulk temperature. Natural convection effects in the annular channel should be quite small, regardless of orientation, if the jacket tube is well insulated. Estimates of uncertainty intervals for Nussult number at various conditions can be found in appendix C.

6. HARDWARE PROCUREMENTS

For all hardware acquisitions that exceeded a cost of $2,500, the standard full and open competitive procurement process was implemented. Once final vendor submissions were received, selection was based on evaluation criteria consisting of a combined cost and technical evaluation basis. Specifications for many of the hardware components have also been developed and procurements initiated. The larger components that were procured include the following:

- Laminar flow meters.
- Gas chiller.
- Test section interior tube.
- Test section jacket.
- Inert gas system.
- Gas compressor or booster pumps.
- Direct current power supplies.

Smaller purchases <$2,500 for items such as tubing, relief valves, fittings, raw materials, vacuum system components, etc., have also been made and are not listed individually.

7. STATUS AT CLOSEOUT AND CONCLUSIONS

This TM has provided an overview and critical evaluation of the test design to date. Conventional relations found in the literature predict that fully developed conditions for turbulent flow should be established over a sizable fraction of the test sections with annulus ratios >0.7. Entrance region effects for turbulent flow will be an important consideration in the interpretation of data for a test section with an annulus ratio of 0.5. Time constants to test section equilibrium should normally be on the order of an hour after a large change in boundary conditions. Several important findings are included in the error analysis contained in appendix C. Below annulus ratios of ≈0.8 error for measured Nusselt number should be less than ±9%. Due to constraints on fabrication tolerances, test section with annulus ratios >0.8 are unlikely to yield well-controlled measurements of Nusselt number. Uncertainty intervals for Nusselt number are expected to correlate only weakly with Reynolds number.

This work might be made to cover a wider range of test conditions and geometrical configurations. These extensions might include different gas mixtures, temperatures, pressures, mass flow rates, annulus ratios, and heat transfer enhancement methods. Every attempt was made in the initial design to permit later accommodation of these contingencies with minimal changes to the basic hardware configuration. In its current embodiment, the apparatus can make accurate heat transfer measurements for circular annuli with an internally heated tube having $0.1 < e < 0.8$. Fabrication tolerances tighter than ASTM standards are required to obtain good data for annuli with $e > 0.8$. Tests of circular tubes ($e = 0$) or circular annuli that are heated on the inner and outer surfaces are also possible by direct heating of the jacket tube. With the existing glass-to-metal power feeds, the test section should be operable near room temperature to at least 250 psia. By active cooling of the feeds and using all welded construction, the current stainless steel test section could be brought to at least 700 °C. Operation at these temperatures requires modification to the inner tube power lead located at the exit of the annulus. For testing He-Ar mixtures, where some gas wastage is tolerable, the RIX compressor should be satisfactory. Tests with He-Xe mixtures will require a booster pump or hermetically sealed turbo blower with very low leakage rates. Cost constraints could justify the building of a liquid nitrogen-cooled trap to recover Xe from the flow loop.

Although this project was terminated prior to setting up the hardware support systems within the laboratory, two of the basic support systems were in fabrication: (1) The test section and (2) the gas circulation loop, both of which may be used to support the future evaluation of heat transfer in gas-cooled core channels. Four test sections for single-channel testing have been designed and one was built using MSFC-directed funds. Engineering of the leak-tight compressor is still required before testing with He-Xe in the loop. Also, design of the connection of the power supplies to the test section still needs to be finalized. The power supplies are currently well within their rated limits. Outside of the length of the gas circulation loop lines, there should be few constraints on the layout of the system.

APPENDIX A—THERMOPHYSICAL PROPERTY FITS

Third-order polynomial fits for thermal conductivity and viscosity of Ar gas with deviations from accepted values over the range 300 K < T < 2,000 K are as follows:

$$k_{\mathrm{Ar}}(T) = 0.0011434 + 6.1189\times10^{-5}T - 2.5315\times10^{-8}T^2 + 5.9271\times10^{-12}T^3\,, \tag{19}$$

with error limits 1.959/–0.414%,

and

$$\mu_{\mathrm{Ar}}(T) = 1.5353\times10^{-6} + 7.8135\times10^{-8}T - 2.2451\times10^{-11}T^2 + 6.643\times10^{-15}T^3\,, \tag{20}$$

with error limits 2.137/–0.677%.

Figures 17 and 18 compare curve fits of the thermal conductivity and dynamic viscosity of Ar as a function of temperature between 100 and 2,000 K to accepted values found in Touloukian. In both cases, third-order polynomial fits were sufficient to capture the data with a maximum deviation of 2%.

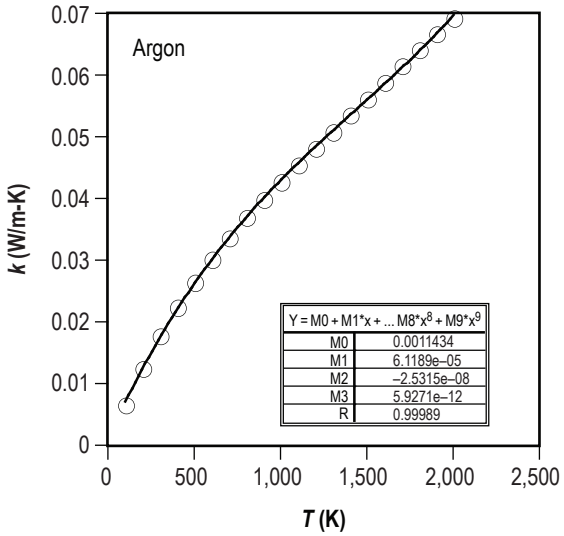

Figure 17. Thermal conductivity of Ar gas at low density: accepted values from Touloukian with third-order polynomial fit.[3]

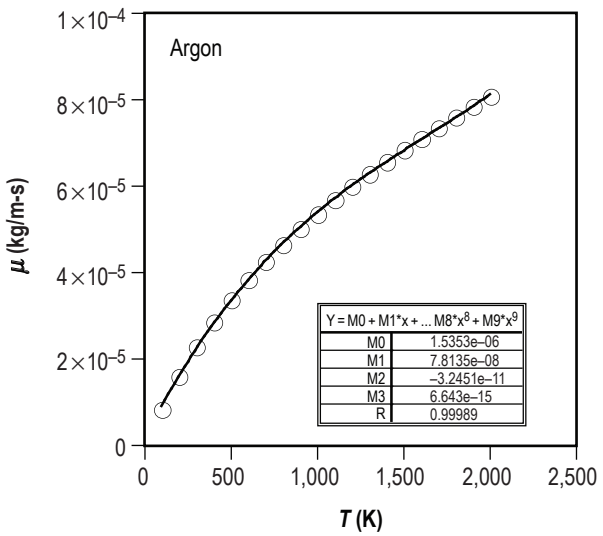

Figure 18. Dynamic viscosity of Ar gas at low density: accepted values from Touloukian with third-order polynomial fit.[4]

Third-order polynomial fits for thermal conductivity and viscosity of He gas with deviations from accepted values over the range 300 K < T < 2,000 K with units W/m-K and kg/m-s, respectively, are as follows:

$$k_{\mathrm{He}}(T) = 0.036953 + 3.9178\times10^{-4}T - 8.1751\times10^{-8}T^2 + 1.5913\times10^{-11}T^3\,, \tag{21}$$

with error limits 1.562/–1.416%,

and

$$\mu_{\mathrm{He}}(T) = 4.693\times10^{-6} + 5.463\times10^{-8}T - 1.7247\times10^{-11}T^2 + 3.159\times10^{-15}T^3\,, \tag{22}$$

with error limits 1.382/–0.434%.

These fits are compared with accepted values in figures 19 and 20.

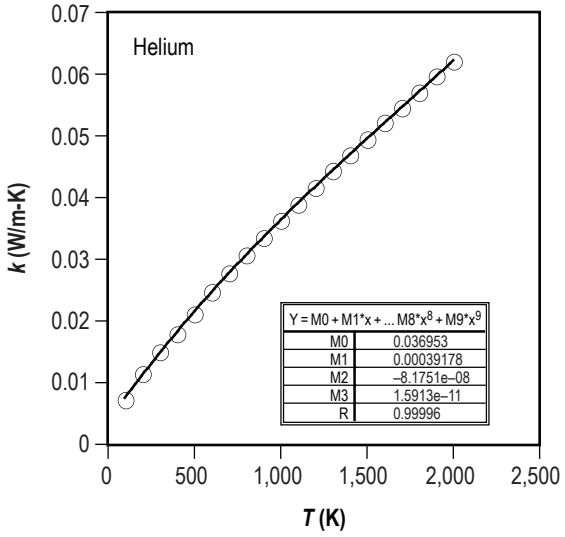

Figure 19. Thermal conductivity of He gas at low density: accepted values from Touloukian with third-order polynomial fit.[3]

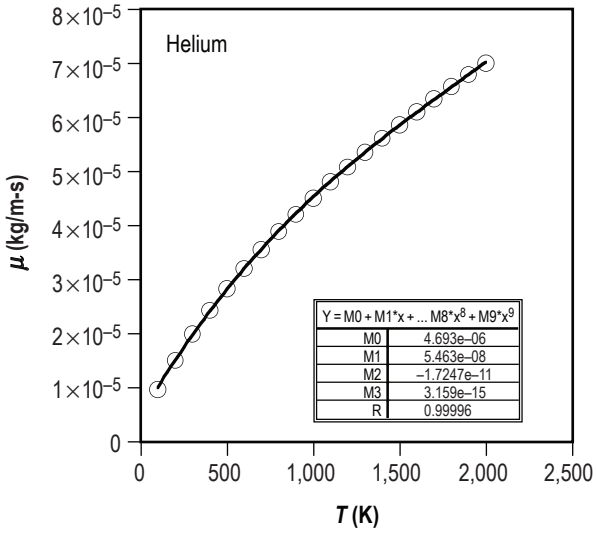

Figure 20. Dynamic viscosity of He gas at low density: accepted values from Touloukian with third-order polynomial fit.[4]

Third-order polynomial fits for thermal conductivity and viscosity of N_2 gas with deviations from accepted values over the range 300 K < T < 2,000 K are

$$k_{\mathrm{N_2}}(T) = 2.7679\times10^{-4} + 9.8753\times10^{-5}T - 5.1554\times10^{-8}T^2 + 1.5427\times10^{-11}T^3\,, \tag{23}$$

with error limits 1.157/–0.434%,

and

$$\mu_{N_2}(T) = 1.9334 \times 10^{-6} + 5.8637 \times 10^{-8} T - 2.5153 \times 10^{-11} T^2 + 5.2386 \times 10^{-15} T^3 , \quad (24)$$

with error limits 2.563 / –0.771%.

Again, the units on temperature are K, and conductivity and viscosity are W/m-K and kg/m-s, respectively. Figures 21 and 22 plot these fits compared to accepted values as a function of temperature.

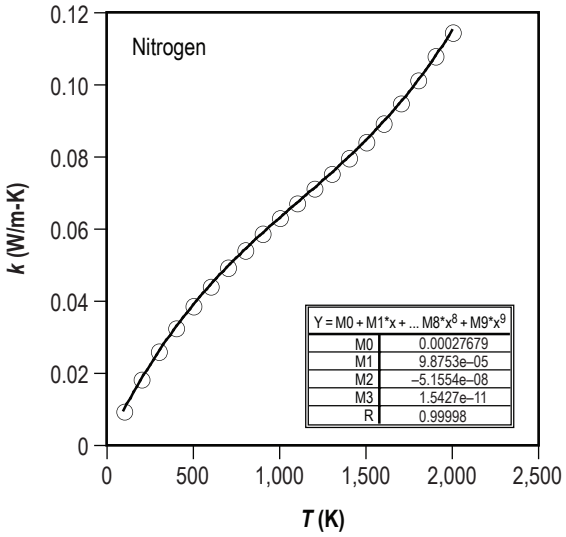

Figure 21. Thermal conductivity of N_2 gas at low density: accepted values from Touloukian with third-order polynomial fit.[3]

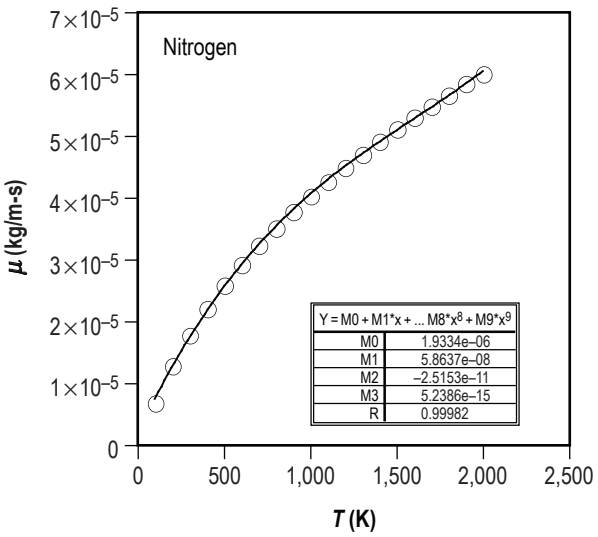

Figure 22. Dynamic viscosity of N_2 gas at low density: accepted values from Touloukian with third-order polynomial fit.[4]

Third-order polynomial fits for thermal conductivity and viscosity of Xe gas with deviations from accepted values over the range 300 K < T < 2,000 K:

$$k_{Xe}(T) = 1.1526 \times 10^{-4} + 1.9695 \times 10^{-5} T - 4.8985 \times 10^{-9} T^2 + 6.5918 \times 10^{-13} T^3 , \quad (25)$$

with error limits 1.157 / –0.434%,

and

$$\mu_{Xe}(T) = -9.921 \times 10^{-7} + 9.0488 \times 10^{-8} T - 3.3146 \times 10^{-11} T^2 + 6.8634 \times 10^{-15} T^3 , \quad (26)$$

with error limits 2.563 / –0.771%.

These fits are compared to accepted values found in the literature in figures 23 and 24.

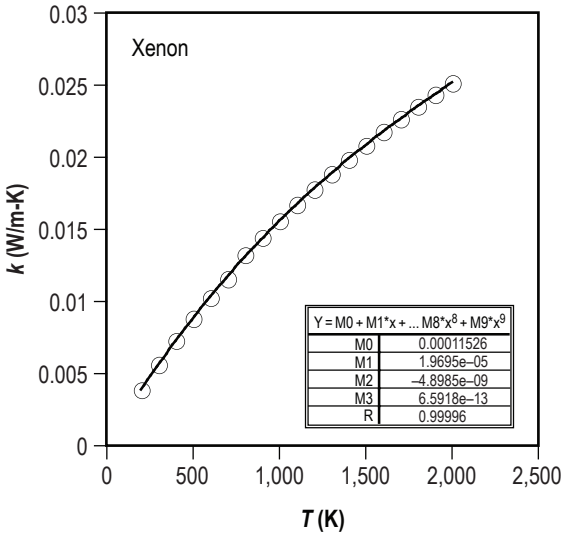

Figure 23. Thermal conductivity of Xe gas at low density: accepted values from Touloukian, Jain, and Jody with third-order polynomial fit.[3,26,27]

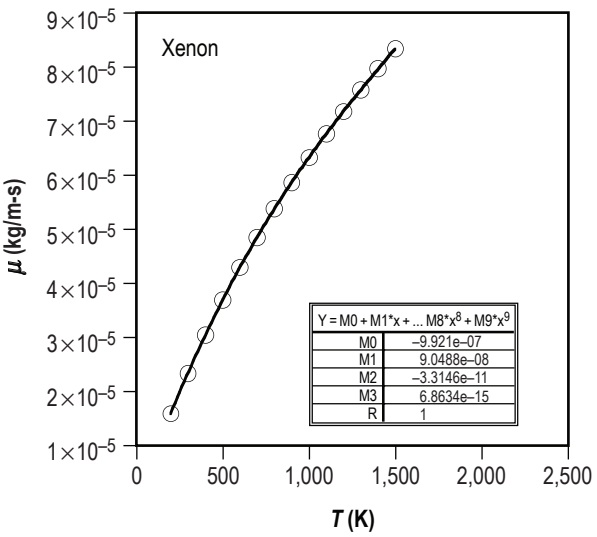

Figure 24. Dynamic viscosity of Xe gas at low density: accepted values from Touloukian with third-order polynomial fit.[4]

Figures 25 and 26 plot deviations for each polynomial curve fit from accepted value as a function of temperature. Above 300 K, deviations in viscosity are generally <1%. Deviations in conductivity are somewhat large, yet above room temperature, stay within a 1.5% band. These deviations are within the test uncertainty cited for the thermal conductivity of gas found in a survey by Ho et al.[28]

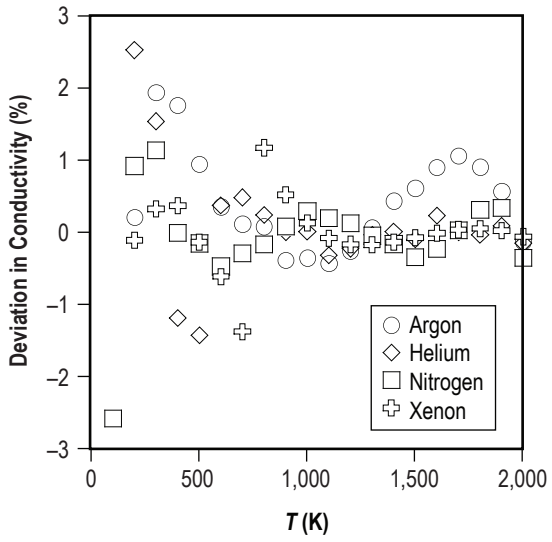

Figure 25. Deviation in third-order thermal conductivity curve fits from accepted values found in Touloukian and Jody.[3,27]

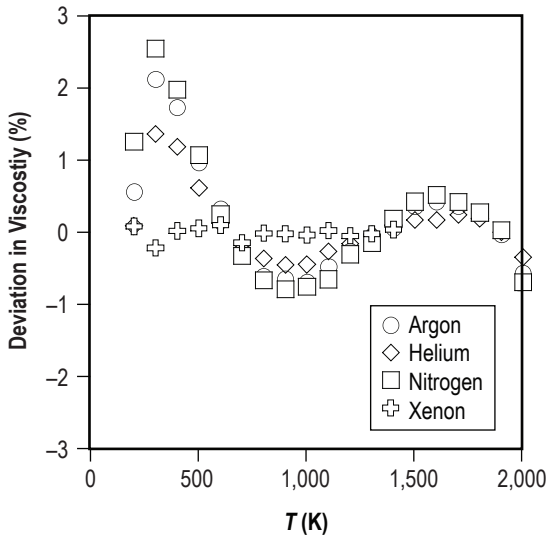

Figure 26. Deviation in third-order dynamic viscosity curve fits from accepted values found in Touloukian and Jody.[4,27]

APPENDIX B—DRAWINGS OF TEST SECTION COMPONENTS

Figures 27–40 show various schematics of the test section components.

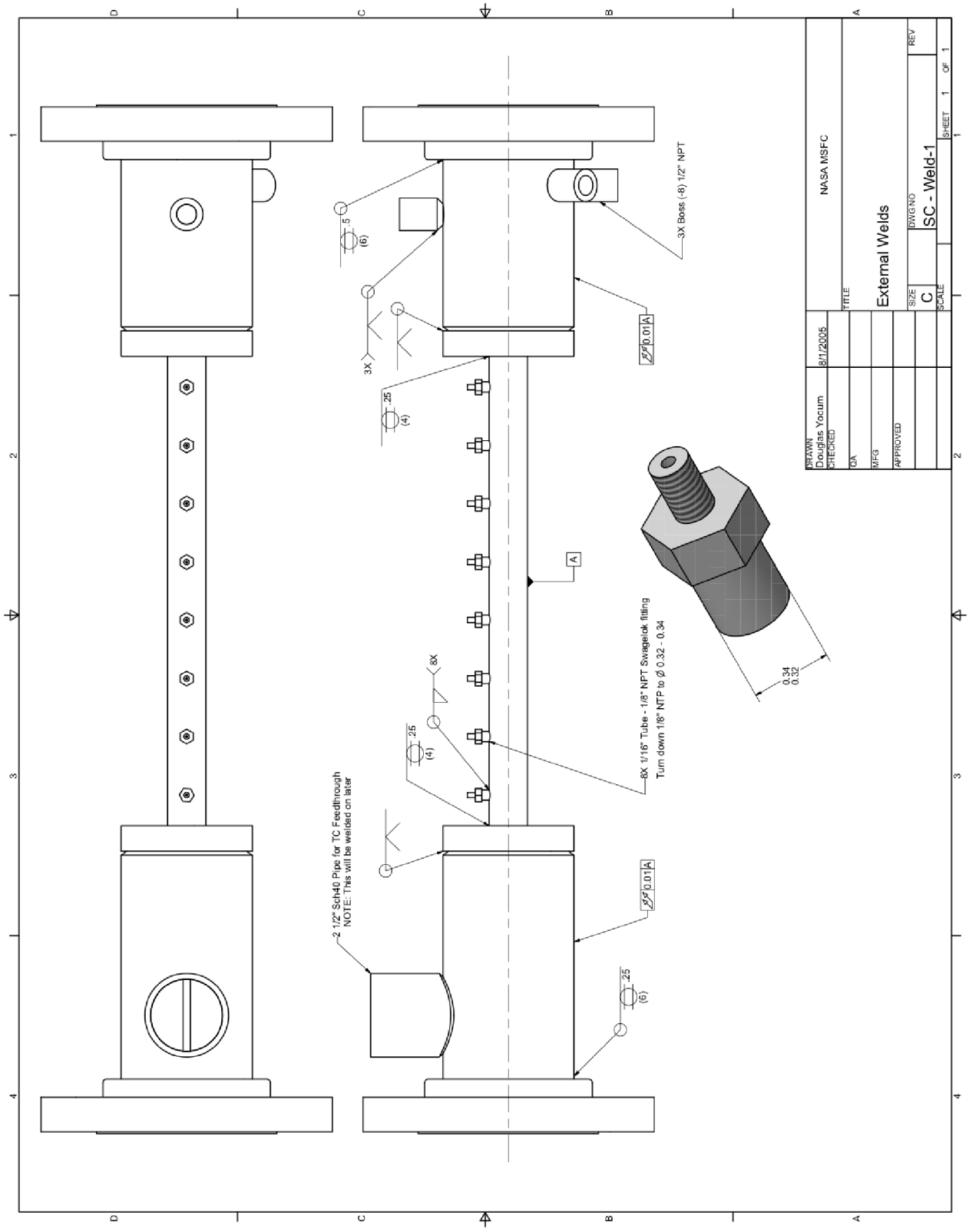

Figure 27. Single-channel test section assembly.

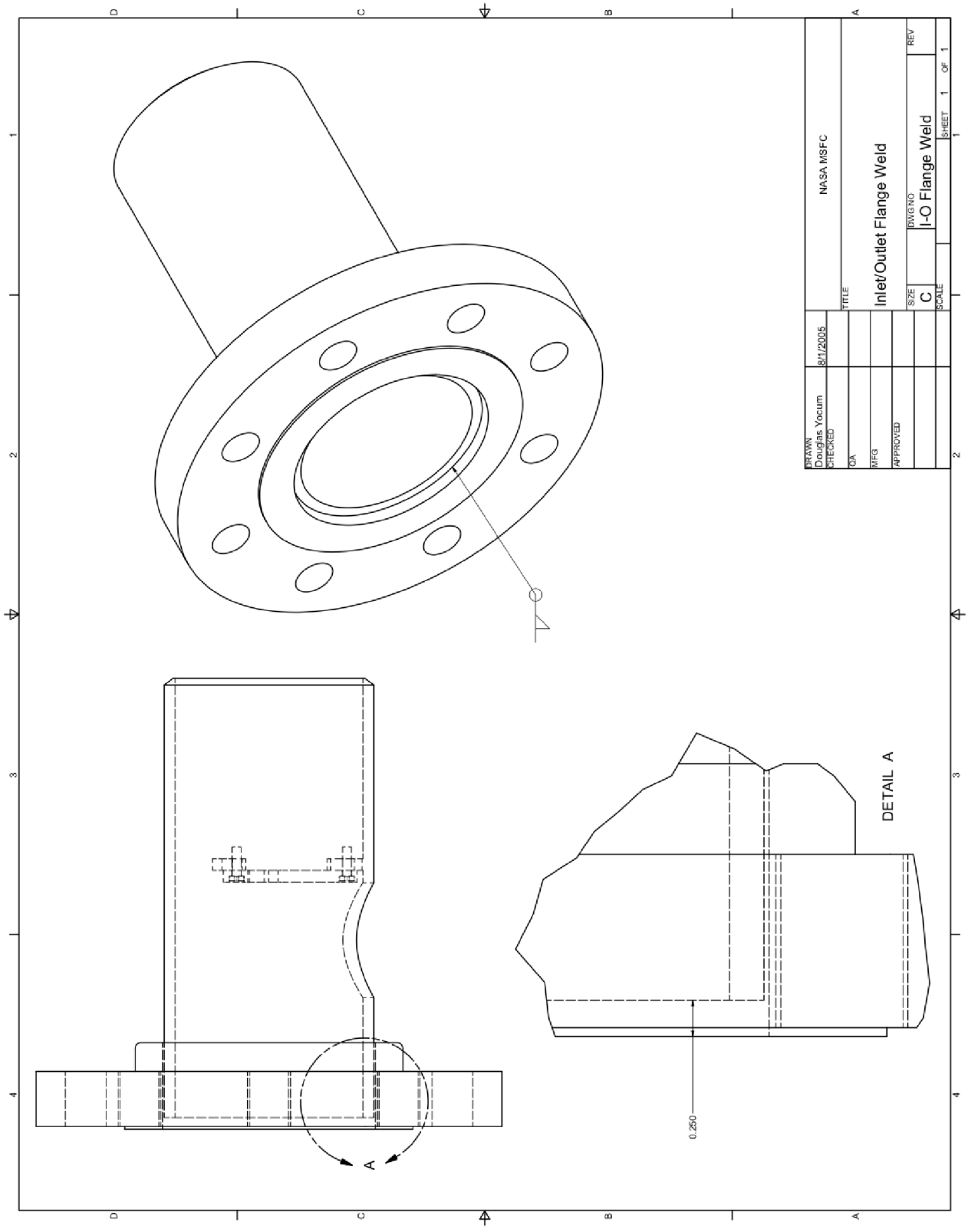

Figure 28. Inlet flange manifold.

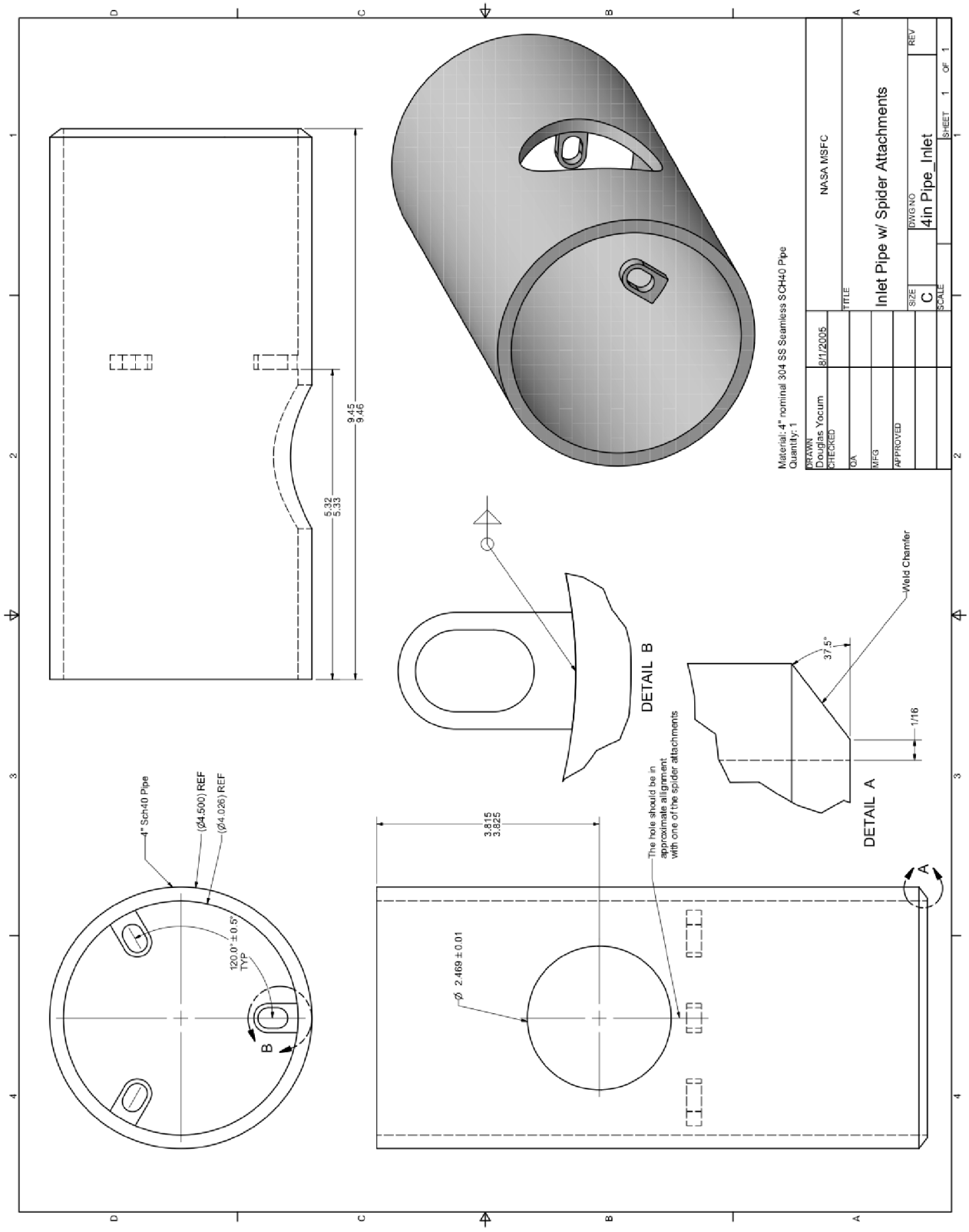

Figure 29. Inlet flange manifold—pipe with spider attachment.

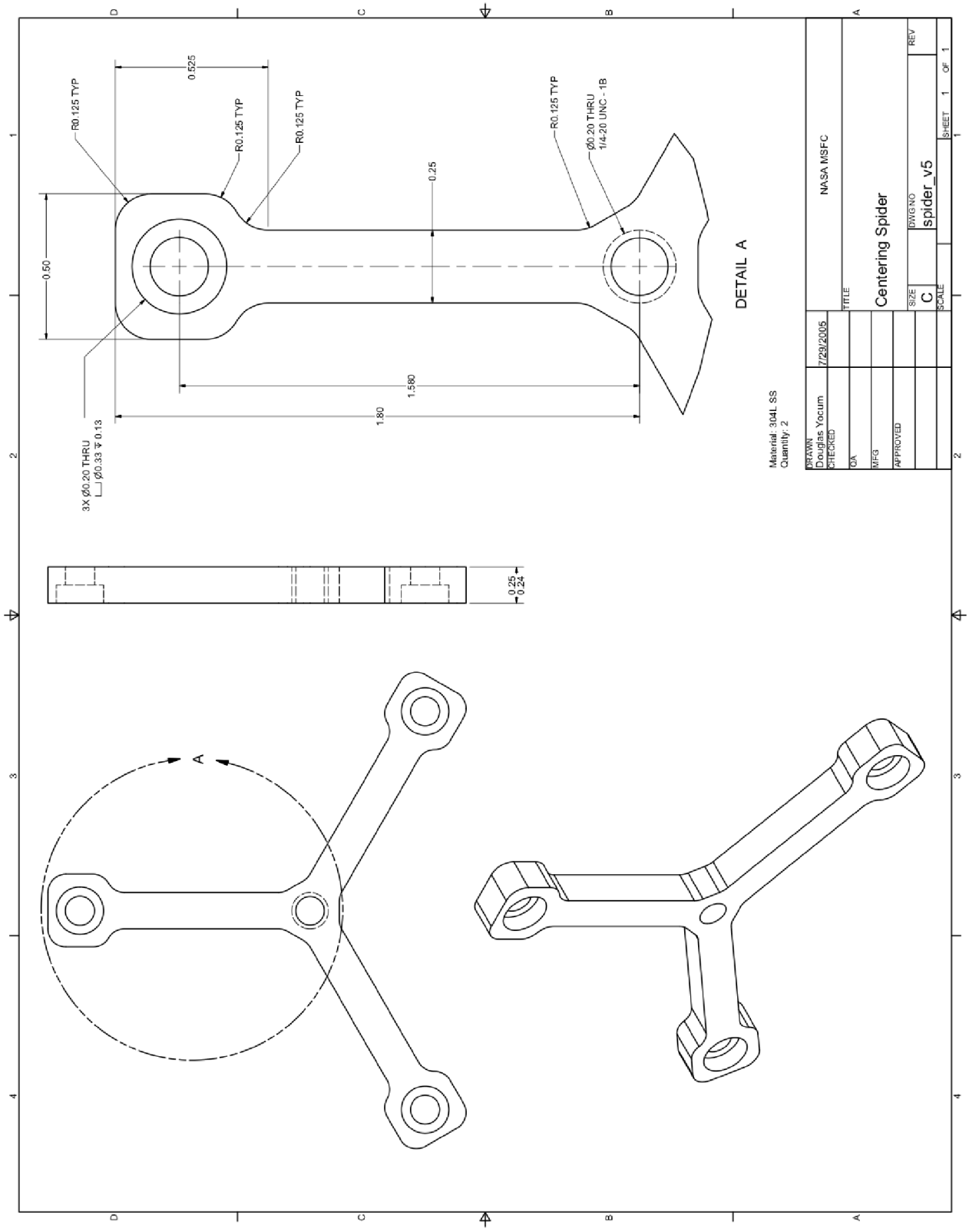

Figure 30. Centering spider.

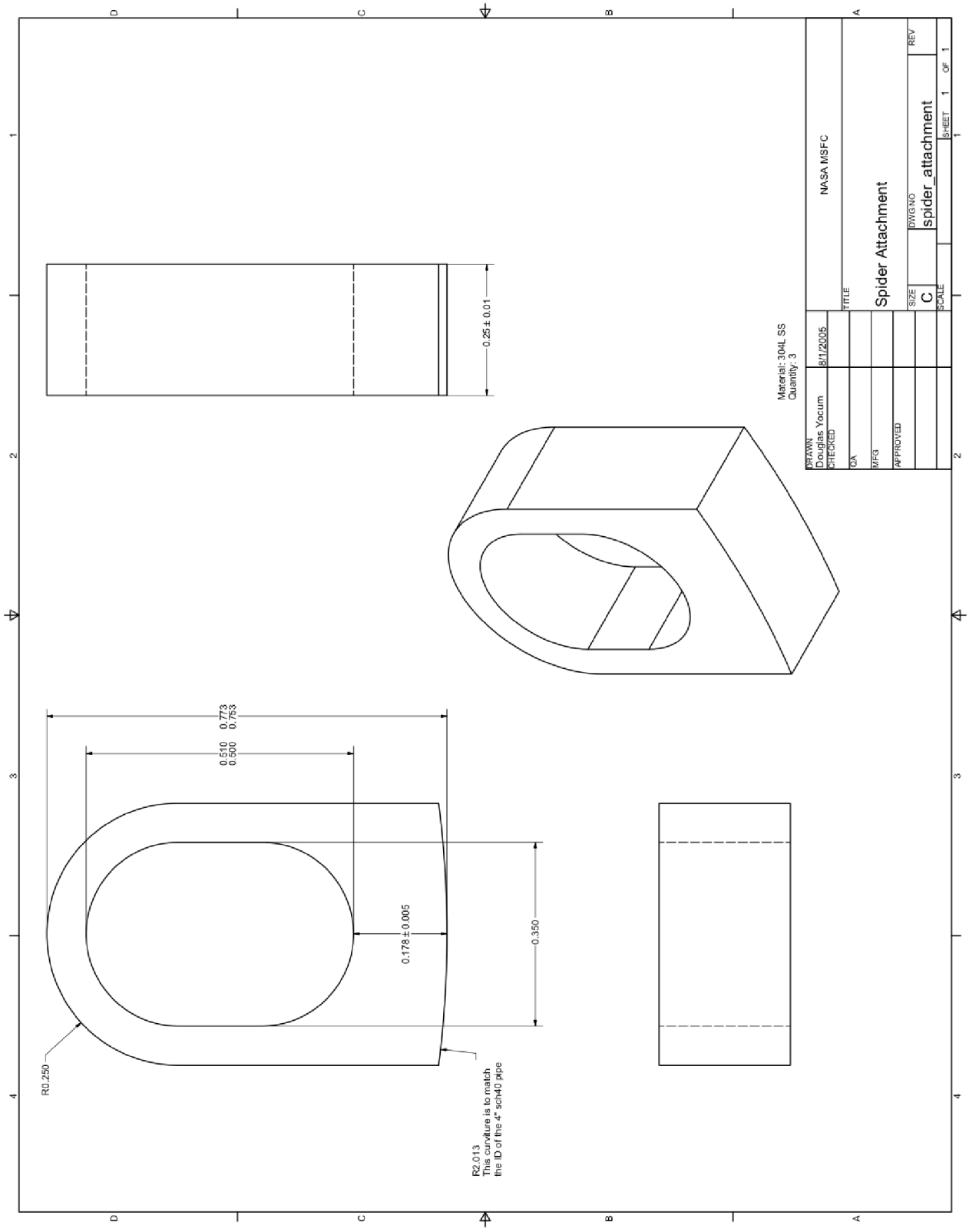

Figure 31. Spider attachment.

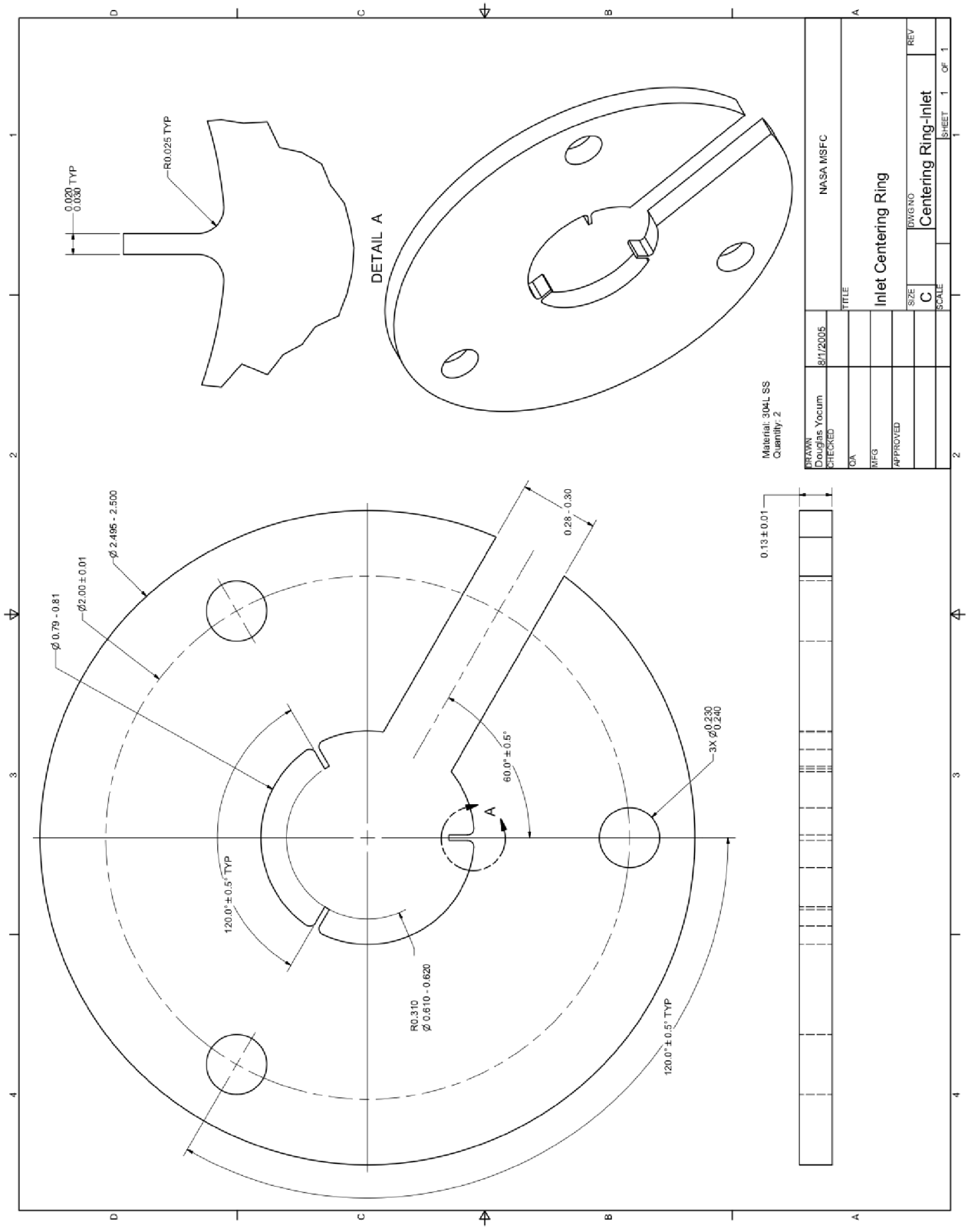

Figure 32. Inlet centering ring.

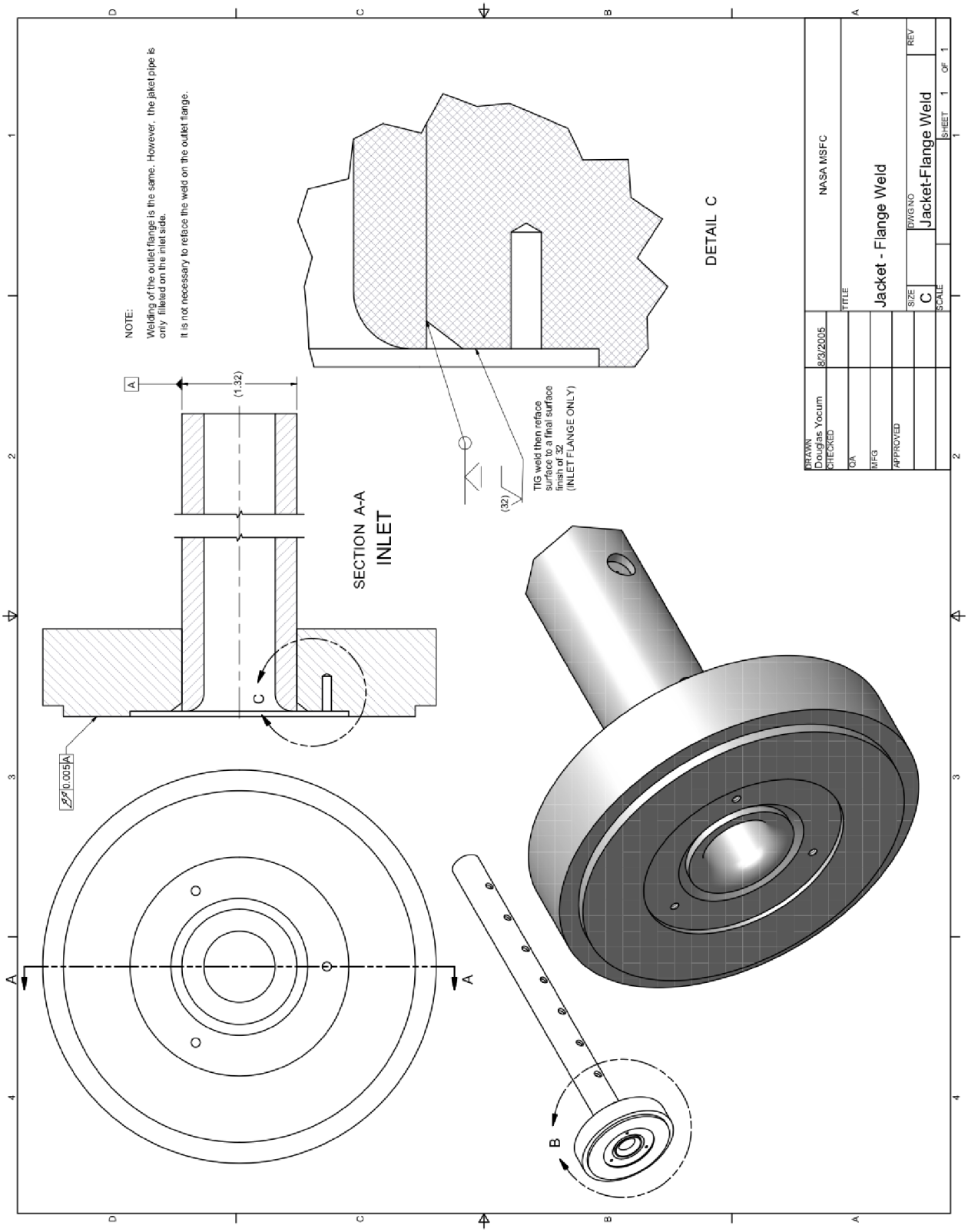

Figure 33. Inlet flange.

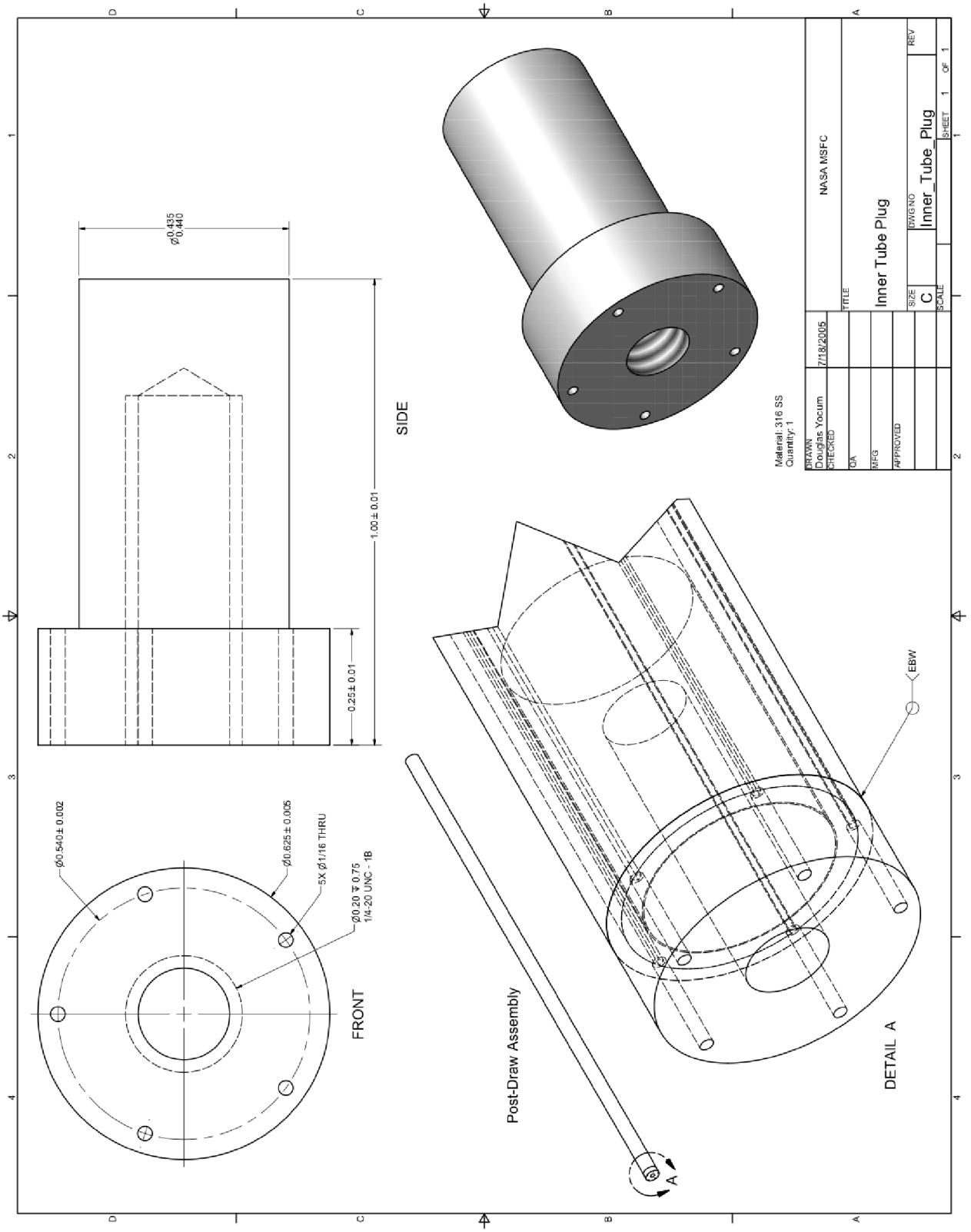

Figure 34. Inner tube plug.

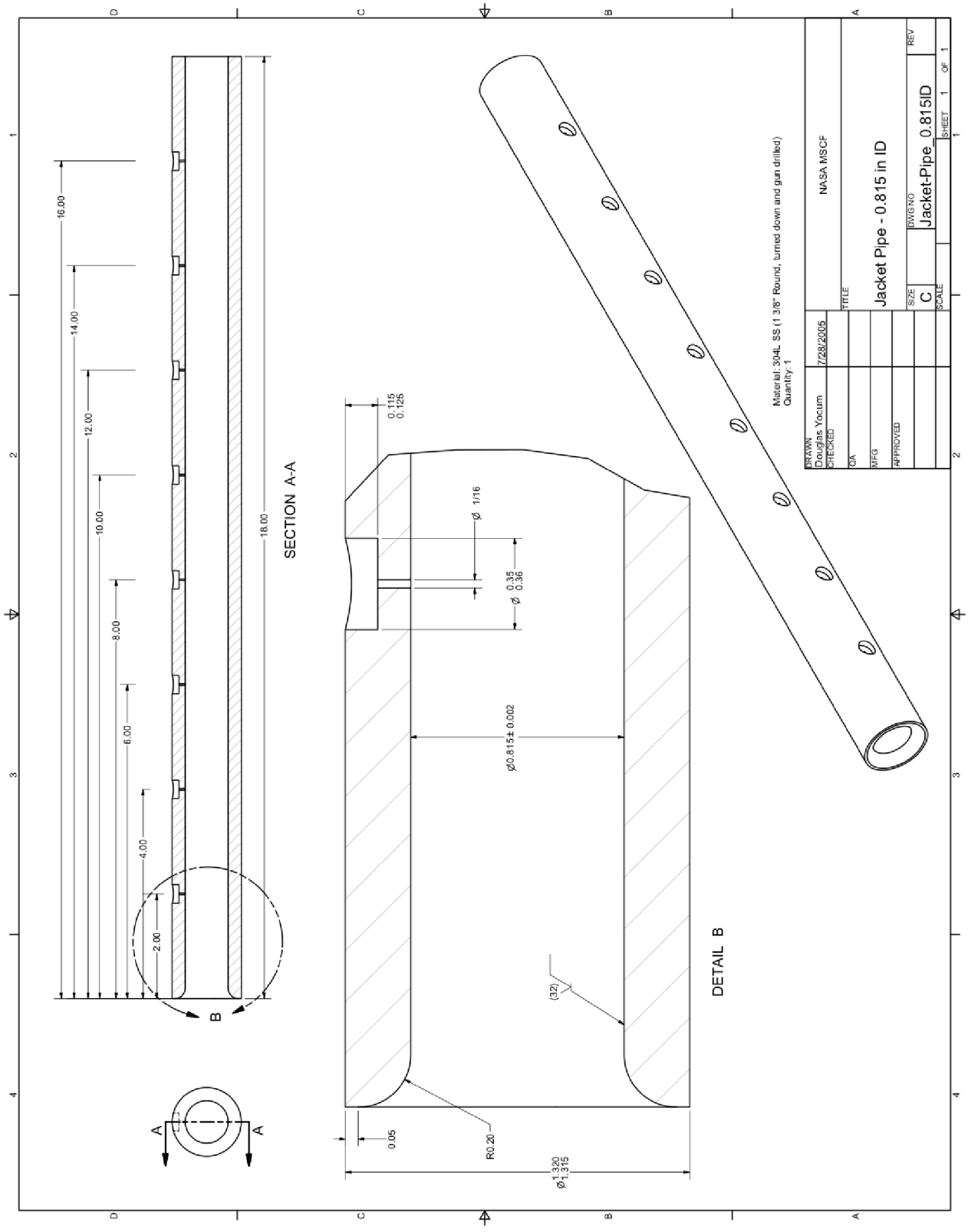

Figure 35. Jacket pipe.

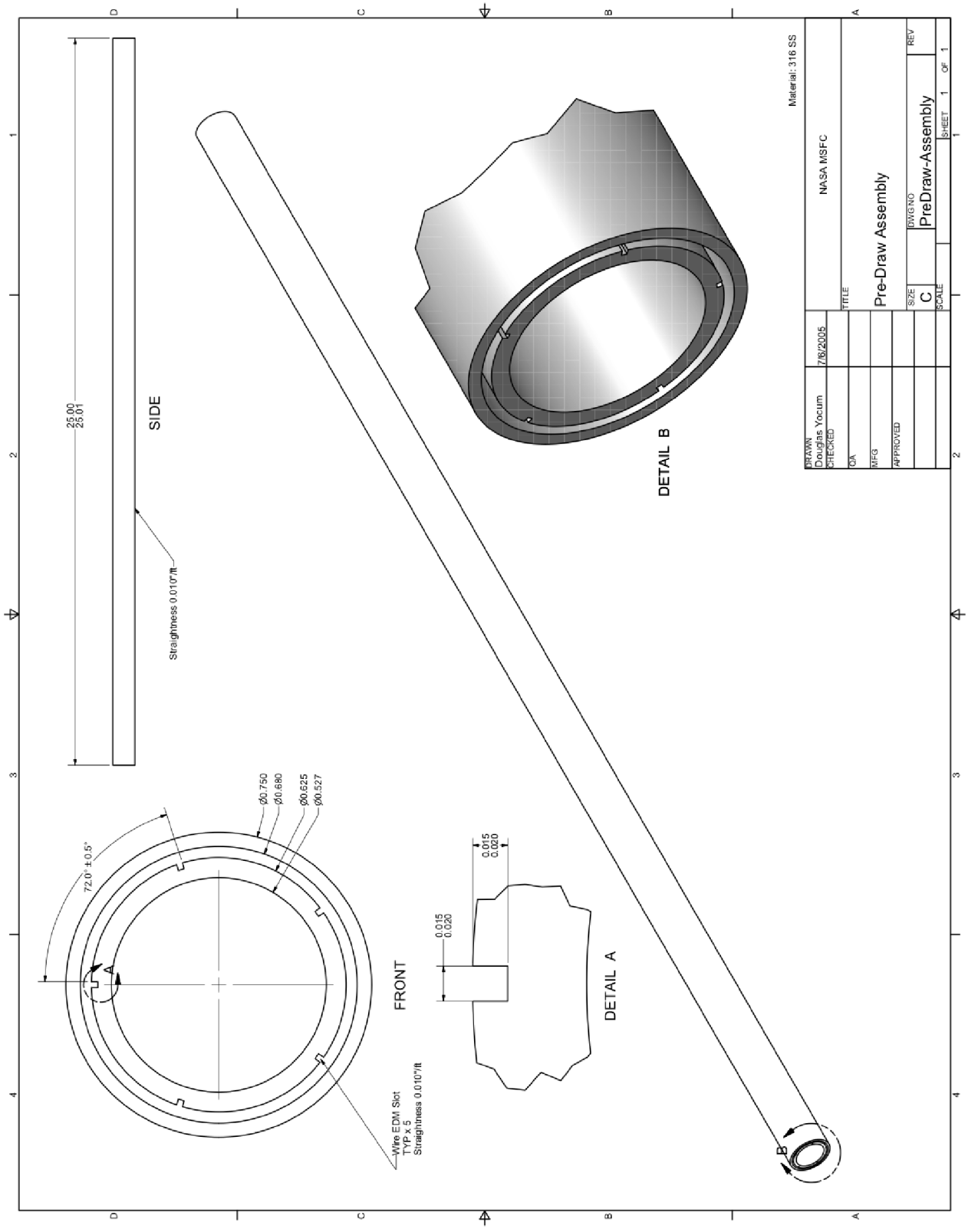

Figure 36. Inner tube predraw assembly.

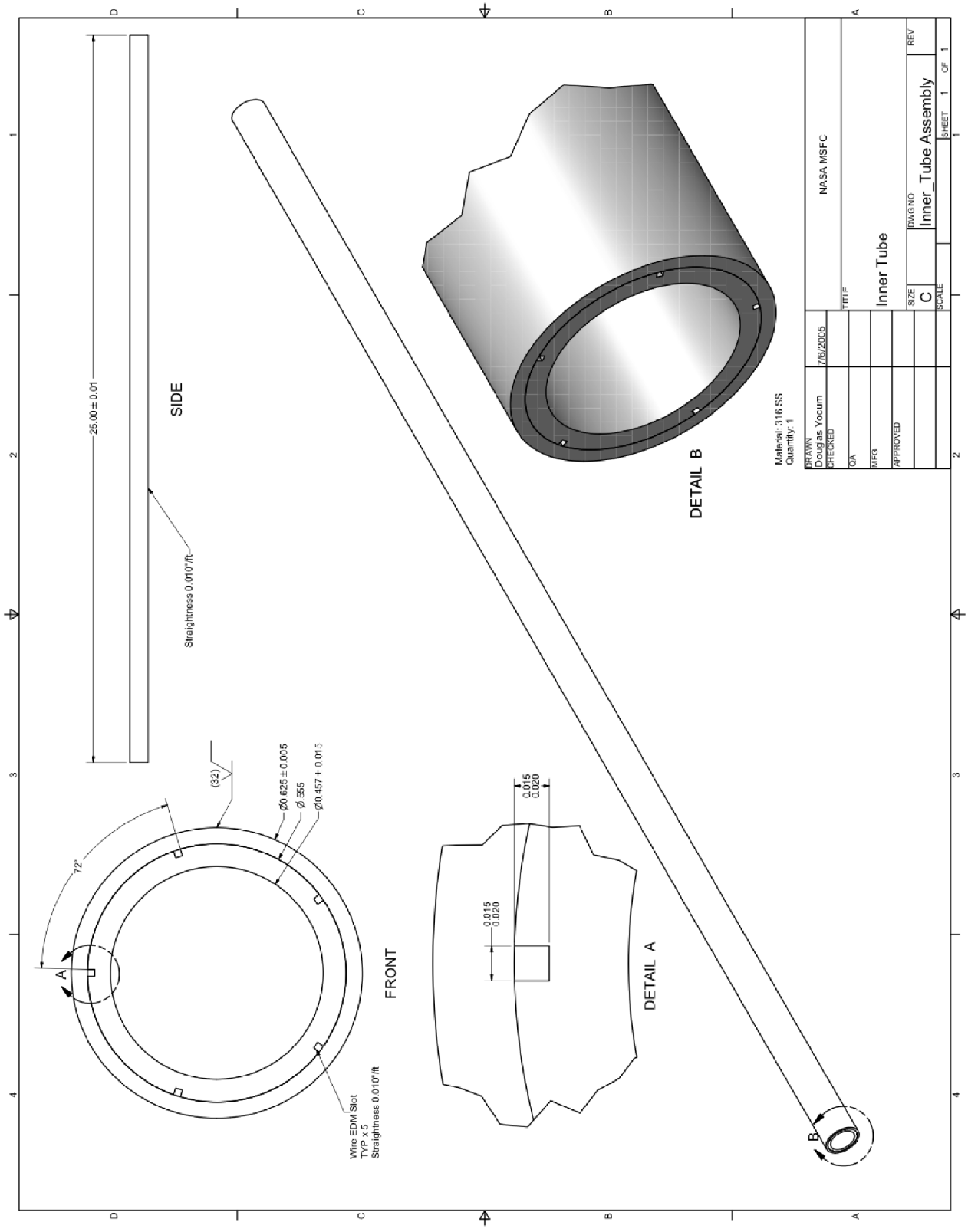

Figure 37. Inner tube postdraw assembly.

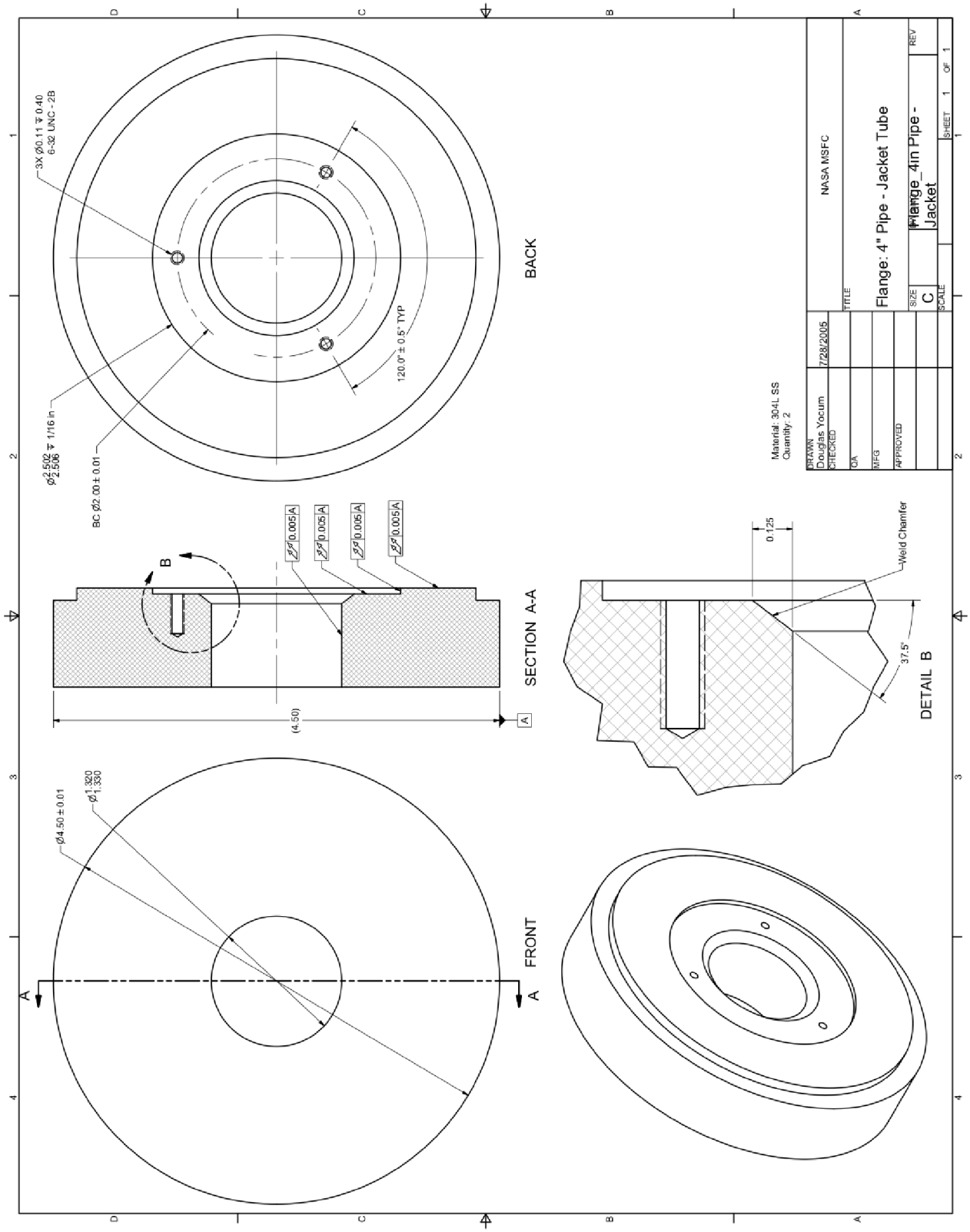

Figure 38. Exit manifold.

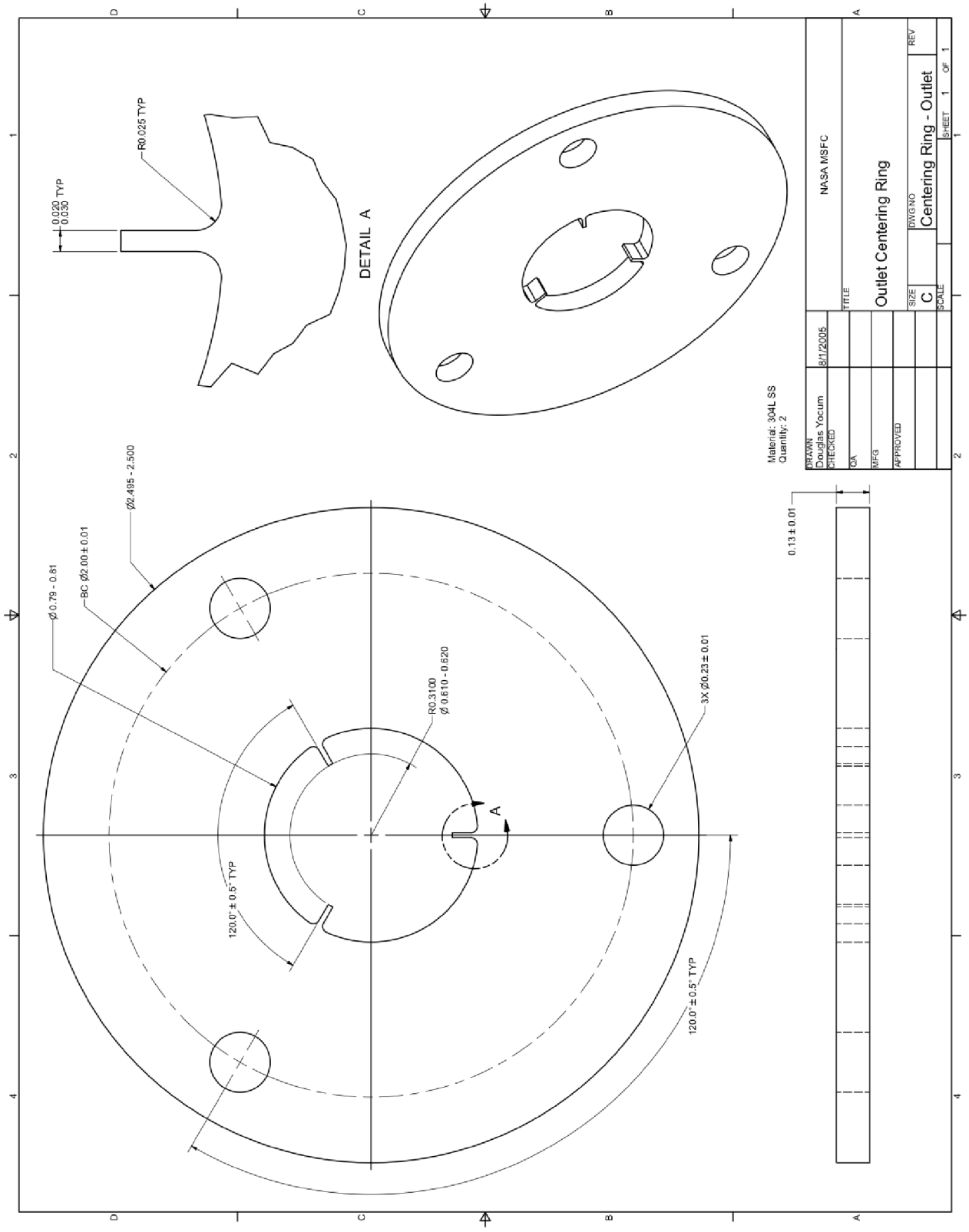

Figure 39. Outlet centering ring.

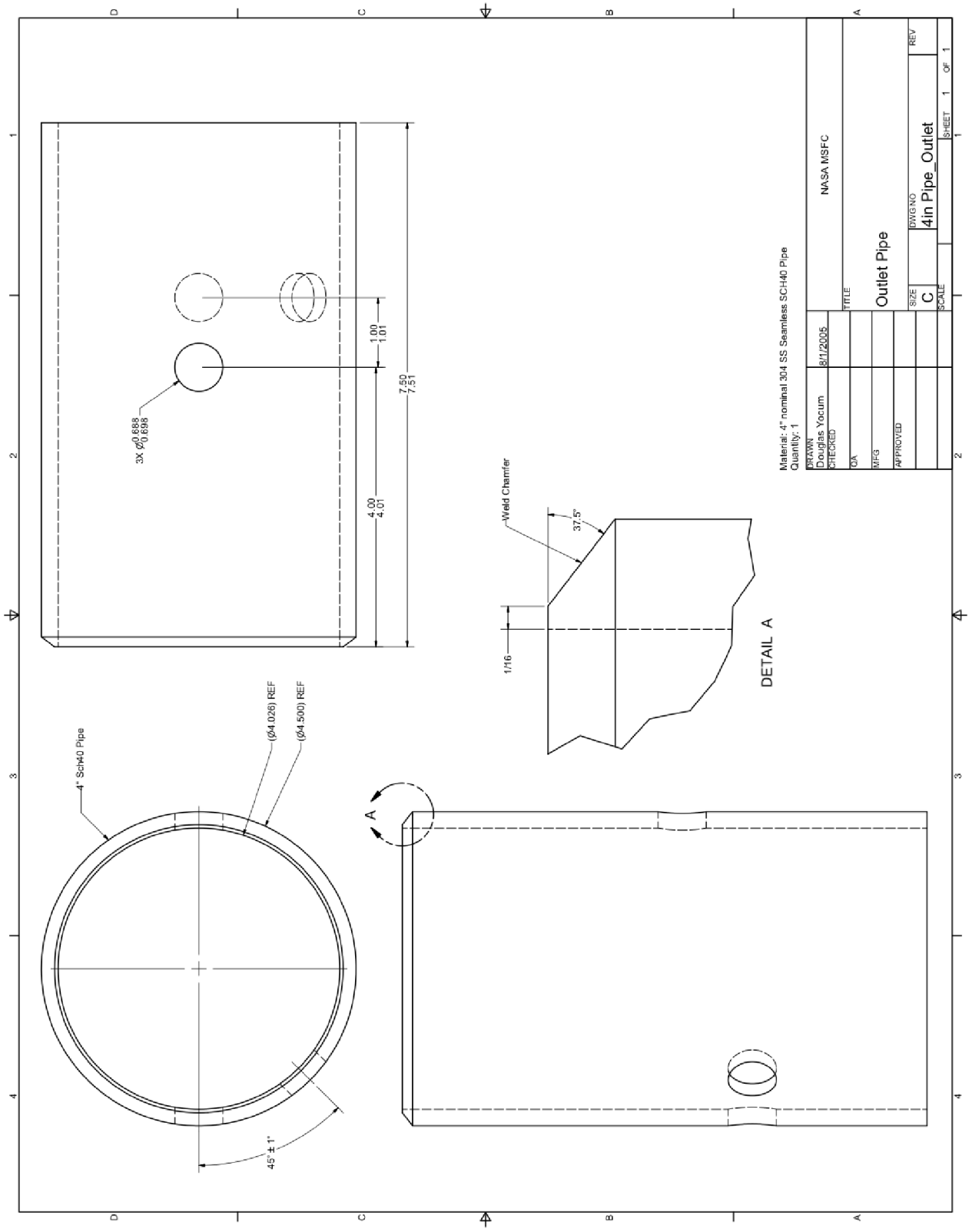

Figure 40. Outlet manifold.

APPENDIX C—TEST UNCERTAINTY ANALYSIS

Given the restrictions on resources, this test series will be predominately single sample with few replicates. In this section, the uncertainty intervals for key results are estimated using the method to describe propagation of uncertainties in single-sample experiments found in Kline and McClintock.[29] Uncertainty intervals are estimated for the independent dimensionless groups Reynolds and Prandtl number and the dependent dimensionless groups they correlate, friction factor, and Nusselt number. Here, all variables that comprise these groups are assumed normally distributed with 20 to 1 odds that the measurement falls within the interval about the mean. Steady-state conditions are assumed for the fully developed region near midpoint of the test section. Uncertainty intervals are calculated for each test section operating near room temperature. The sensitivity of these estimated uncertainty intervals to variations in test conditions, such as temperature and Reynolds number, is also examined.

C.1 Prandtl Number Uncertainty

The Prandtl number, $Pr = \mu c_p/k$, of the gas is used here as an independent variable in the correlation of the nondimensional heat transfer rate. It is a function of specific heat—a thermodynamic property, and also viscosity and thermal conductivity—both transport properties. The shape of the Prandtl number versus composition curve for He-Ar mixtures is shown in the introductory paragraphs of this TM. Prandtl number is generally a weak function of temperature and, near its minima, a weak function of composition. Given these relations, the variation of Prandtl number should be insensitive to small variations in temperature and composition. The same does not hold for the variables that comprise Prandtl number. Gas viscosity and thermal conductivity depend on temperature and composition. Ideal gas specific heat depends on composition only. Viscosity and thermal conductivity correlations agree with data for He-Ar gas mixtures reported to the 1% and 4% levels, respectively, over the range of conditions considered here. Property correlations using such published values should be accurate to these levels for a given temperature or composition. The associated uncertainty interval is

$$\left(\frac{\delta Pr}{Pr}\right)^2 = \left(\frac{\delta \mu}{\mu}\right)^2 + \left(\frac{\delta c_p}{c_p}\right)^2 + \left(\frac{\delta k}{k}\right)^2 = 0.01^2 + 0.01^2 + 0.04^2 = 0.0424 \ , \tag{27}$$

where the uncertainty intervals for viscosity and temperature are estimated based on agreement between correlation and data. The uncertainty interval for specific heat is estimated based on possible gas composition errors. To reduce the chance of inadvertent contamination, the test section will be evacuated $<10^{-6}$ torr before premixed, high-pressure gas is added. The composition of bottles containing He-Ar mixtures is typically known to the part-per-million level. For this estimate, gas composition will be assumed known to within 1%. This rough estimate yields a value of Prandtl number near the He-Ar compositional minima of $Pr = 0.39 \pm 0.017$ (20 to 1 odds).

C.2 Friction Factor Uncertainty for Adiabatic Flows

The friction factor for fully developed turbulent flow through an annulus is a weak function of eccentricity when $e^* \rightarrow 0$.[8] Since it is possible that friction factor measurements will not be made on a heated test section, applied power and temperature rise through the test section cannot be relied upon to establish the flow condition. Instead, a laminar flow meter provides the mass flow rate measurement for the adiabatic case. The friction factor for adiabatic flows between two points along the length of the test section can be described as $f = 2\Delta p(\Delta x)^{-1}A^2V^{-2}\rho^{-1}d_h$. The resulting uncertainty interval for friction factor in terms of these variables is:

$$\left(\frac{\delta f}{f}\right)^2 = \left(\frac{\delta \Delta p}{\Delta p}\right)^2 + \left(\frac{\delta \Delta x}{\Delta x}\right)^2 + \left(\frac{2\delta A}{A}\right)^2 + \left(\frac{-2\delta V}{V}\right)^2 + \left(\frac{\delta \rho}{\rho}\right)^2 + \left(\frac{\delta d_h}{d_h}\right)^2 \quad . \tag{28}$$

Pressure taps are placed at eight locations along the test section at 5.08-cm intervals. A Pressure Systems Esterline model 9116 network analyzer senses differential pressure at each tap with respect to a reference port located near the center of the test section. The manufacturer quotes a measurement resolution of ±0.003% full scale, a static accuracy of ±0.15% full scale for $p < 20$ kPa, and ±0.05% full scale for $p > 20$ kPa. Total thermal error is ±0.0015% full scale per degrees Celsius for $p < 20$ kPa and ±0.001% full scale per degrees Celsius for $p > 20$ kPa. The line pressure effect for this sensor is ±0.0003% full scale per psi for absolute $p > 100$ kPa. If the pressure drop between taps is assumed <20 kPa and thermal error is taken to be 20 °C, the relative uncertainty for a 7-kPa, full-scale sensor measuring a 224 Pa reading is

$$\frac{\delta \Delta p}{\Delta p} = \frac{7{,}000\ Pa}{224\ Pa}\left[\left(\frac{0.153}{100}\right)^2 + \left(\frac{0.0015}{100}\,\frac{1}{°\mathrm{C}}\,20\ °\mathrm{C}\right)^2 + \left(\frac{0.0003}{100}\,\frac{1}{\mathrm{psi}}\,100\mathrm{psi}\right)^2\right]^{0.5} = 0.0496 \quad . \tag{29}$$

The uncertainty interval for the 2-in spacing between pressure taps is taken from tolerances on the fabrication drawings:

$$\frac{\delta \Delta x}{\Delta x} = \frac{0.010}{2} = 0.005 \, . \tag{30}$$

The uncertainty interval for the channel cross-sectional area, $A = \pi\left(D_i^2 - d_o^2\right)/4$ are taken from the fabrication drawings:

$$\frac{\delta A}{A} = \left[\left(\frac{\delta D_i}{D_i}\right)^2 + \left(\frac{\delta d_o}{d_o}\right)^2\right]^{0.5} = \left[\left(\frac{0.002}{0.815}\right)^2 + \left(\frac{0.005}{0.625}\right)^2\right]^{0.5} = 0.00886 \quad . \tag{31}$$

Table 7 shows estimated uncertainty for adiabatic friction factors for He-40%Ar near room temperature based on an assumed Blasius-type friction factor correlation. The second column in the table

contains the values used to compute uncertainty in the column labeled AF2. The estimates for AF1, AF2, and AF3 use Esterline sensors with 7-kPa full scale. For AF4, a 2-kPa, full-scale sensor is used. For low annulus ratio, AF4, the pressure drop is quite low and the sensitivity of the pressure transducer dominates uncertainties that approach 30%. As the annulus ratio increases, uncertainties in gas density and hydraulic diameter become important. The uncertainty for these remaining cases, with 20 to 1 odds, is under 6%. Table 8 shows the influence of Reynolds number on uncertainty in pressure drop measurement. More sensitive pressure transducers will be needed if accurate readings are desired at $Re < 10{,}000$.

Table 7. Uncertainties in friction factor measurement for $r^* = 0.76$, He-40%Ar.

Symbol	Value	Unit	Description	AF2
P	689,303	Pa	Absolute pressure	0.0007
Δp	303	Pa	Pressure drop	0.0367
Δx	2	in	Spacing between pressure taps	0.005
ρ_s	5.237	kg/m^3	Gas density	0.0203
m	0.0144	kg/s	Mass flow rate	0.0086
A_c	0.2148	in^2	Cross-sectional area	0.0084
d_h	0.19	in	Hydraulic diameter	0.0186
Re	30,000	–	Reynolds number	0.0431
f	0.007	–	Friction factor correlation	0.052

Table 8. Uncertainties in friction factor measurement for He-40%Ar mixtures.

Re (r^*)	0.83	0.76	0.71	0.5
3,000	0.344	1.201	2.73	15.2
7,000	0.089	0.275	0.622	3.46
15,000	0.047	0.089	0.167	0.91
22,000	0.044	0.052	0.091	0.47
30,000	0.043	0.052	0.06	0.27

C.3 Nusselt Number Uncertainty

The test section is assumed sufficiently insulated to keep heat loss a small fraction of the applied power. An electrically heated tube provides power to the test section for the single-channel heat transfer test. This power is determined using measurement of voltage across the test section terminals and the voltage across a known resistance in the circuit. From Rohsenow, Hartnett, and Ganic,[8] a simple linear relation between Nusselt number and eccentricity can be assumed, provided the annulus ratio is <0.8. Expressing Nusselt number in this way produces the following formulation:

$$Nu = \frac{q d_h \left(1 - e/2\right)}{A\left(T_w - T_g\right) k_g} \quad , \tag{32}$$

where k_g is the thermal conductivity of the gas, d_h is the hydraulic diameter of the test section, q/A is the power supplied per unit area supplied to the gas locally, T_w is the measured wall temperature, T_g is the

gas bulk temperature, and e is the eccentricity of the annulus. The temperature difference is based on the reading of wall thermocouples, with accuracy on the order of $\pm$1.1 °C. Gas properties are assessed based on methods outlined earlier in this TM at the local temperature. Natural convection effects in the annular channel should be quite small, regardless of orientation, since the jacket tube is well insulated.

C.3.1 General Uncertainty Equations

For the current uncertainty analysis, the expression in equation (32) is used and the Nusselt number can be expressed as a function of the following terms:

$$Nu = f(q, A, d_h, T_w, T_g, k_g, e) \ . \tag{33}$$

The linear propagation of errors results in

$$\delta Nu = \frac{\partial Nu}{\partial q}\delta q + \frac{\partial Nu}{\partial A}\delta A + \frac{\partial Nu}{\partial d_h}\delta d_h + \frac{\partial Nu}{\partial T_w}\delta T_w + \frac{\partial Nu}{\partial T_g}\delta T_g + \frac{\partial Nu}{\partial k_g}\delta k_g + \frac{\partial Nu}{\partial e}\delta e \ . \tag{34}$$

Squaring, expanding, and setting all correlated terms to zero results in the final expression:

$$\begin{aligned}\delta Nu^2 = &\left(\frac{\partial Nu}{\partial q}\right)^2 \delta q^2 + \left(\frac{\partial Nu}{\partial A}\right)^2 \delta A^2 + \left(\frac{\partial Nu}{\partial d_h}\right)^2 \delta d_h^2 + \left(\frac{\partial Nu}{\partial T_w}\right)^2 \delta {T_w}^2 \\ &+ \left(\frac{\partial Nu}{\partial T_g}\right)^2 \delta {T_g}^2 + \left(\frac{\partial Nu}{\partial k_g}\right)^2 \delta k_g^2 + \left(\frac{\partial Nu}{\partial e}\right)^2 \delta e^2 \ .\end{aligned} \tag{35}$$

All partial derivatives listed in equation (35) are as follows:

$$\frac{\partial Nu}{\partial q} = \frac{d_h\left(1 - e/2\right)}{A\left(T_w - T_g\right)k_g} \ , \tag{36}$$

$$\frac{\partial Nu}{\partial A} = -\frac{q d_h\left(1 - e/2\right)}{A^2\left(T_w - T_g\right)k_g} \ , \tag{37}$$

$$\frac{\partial Nu}{\partial d_h} = \frac{q\left(1 - e/2\right)}{A\left(T_w - T_g\right)k_g} \ , \tag{38}$$

$$\frac{\partial Nu}{\partial T_w} = -\frac{q d_h\left(1 - e/2\right)}{A\left(T_w - T_g\right)^2 k_g} \ , \tag{39}$$

$$\frac{\partial Nu}{\partial T_g} = \frac{q d_h \left(1 - e/2\right)}{A\left(T_w - T_g\right)^2 k_g} \quad , \tag{40}$$

$$\frac{\partial Nu}{\partial k_g} = -\frac{q d_h \left(1 - e/2\right)}{A\left(T_w - T_g\right) k_g^2} \quad , \tag{41}$$

and

$$\frac{\partial Nu}{\partial e} = -\frac{1}{2}\frac{q d_h}{A\left(T_w - T_g\right) k_g} \quad . \tag{42}$$

Substituting equations (36)–(42) into equation (35) and rearranging each derivative term by dividing it by its square results in the following:

$$\delta Nu^2 = \left(\frac{q d_h \left(1 - e/2\right)}{A\left(T_w - T_g\right) k_g}\right)^2 \left[\left(\frac{\delta q}{q}\right)^2 + \left(\frac{\delta d_h}{d_h}\right)^2 + \left(\frac{\delta A}{A}\right)^2 + \left(\frac{-\delta T_w}{\left(T_w - T_g\right)}\right)^2\right.$$

$$\left. + \left(\frac{\delta T_g}{\left(T_w - T_g\right)}\right)^2 + \left(\frac{\delta k_g}{k_g}\right)^2 + \left(\frac{-\delta e}{2\left(1 - e/2\right)}\right)^2\right] . \tag{43}$$

Each of the terms in equation (43) must now be determined.

C.3.2 Heating Rate Uncertainty Interval

The heating rate is established assuming electrical power is uniformly dissipated to the inner tube with homogeneous composition and cross section. Additional heating or cooling can occur from parasitic losses across insulation that couples the test section gas and the environment:

$$q = EI - \frac{2\pi k_g L\left(T_g - T_\infty\right)}{\ln\left(D_s / D_o\right)} \quad . \tag{44}$$

A layer of 0.068-W/m-K insulation ≈2.3 in thick on a 1-in-diameter tube is sufficient to keep the second parasitic term to <4 W. The uncertainty interval is

$$\delta q^2 = \left(\frac{\partial q}{\partial E}\right)^2 \delta E^2 + \left(\frac{\partial q}{\partial I}\right)^2 \delta I^2 + \delta q_o{}^2 \, . \tag{45}$$

The nominal current through the test section is 1,500 A ± (0.13/100 1,500) A as measured with a high-precision resistor. The terminal voltage is 0.5 V ± (0.03/100 0.5) V. The thermal loss from the test section assumes use of vermiculite, or similar packed or loose-packed insulation, and an overall temperature gradient between the gas and ambient established at the entrance of the test section:

$$\delta q^2 = I^2 \delta E^2 + E^2 \delta I^2 + \delta q_o^2 = \left(1{,}500 \times 0.15 \times 10^{-4}\right)^2 + \left(0.5 \times 1.95\right)^2 + 3.7^2 \tag{46}$$

or

$$q = 888 \pm 4.05 \text{ W (20 to 1)} \ . \tag{47}$$

C.3.3 Hydraulic Diameter Uncertainty Interval

The hydraulic diameter, d, uncertainty interval is estimated using fabrication tolerance:

$$d_h = D_i - d_o \ , \tag{48}$$

$$\left(\delta d_h\right)^2 = \left(\delta D_i\right)^2 + \left(\delta d_o\right)^2 = \left(0.005\right)^2 + \left(0.002\right)^2 , \tag{49}$$

or

$$d = 0.19 \pm 0.00539 \text{ in (20 to 1)} \ . \tag{50}$$

C.3.4 Heat Transfer Area Uncertainty Interval

Power is generated at a uniform rate in the inner tube by electrical dissipation. The convective heat flux is based on the wetted area of the inner tube given by $A = \pi d_o L$, where the length is along the test section enclosed by the jacket:

$$\left(\delta A\right)^2 = \left(\frac{\partial A}{\partial d_o}\delta d_o\right)^2 + \left(\frac{\partial A}{\partial L}\delta L\right)^2 = \left(\pi \times 18 \times 0.005\right)^2 + \left(\pi \times 0.625 \times 0.10\right)^2 \tag{51}$$

or

$$A = 35.3 \pm 0.344 \text{ in}^2 \text{ (20 to 1)} \ . \tag{52}$$

C.3.5 Surface Temperature Uncertainty Interval

Surface temperatures are measured with a thermocouple embedded into the wall of the electrically heated inner tube. To get an accurate reading, the measurement must be corrected for the temperature drop between the thermocouple and the surface, assuming the region around the thermocouple and the cooled surface can be approximated as a plane wall with uniform energy generation per unit volume, adiabatic on one face and convectively cooled on another. The surface temperature is related to the thermocouple temperature by

$$T_w = T_t - \frac{q'''R^2}{2k_s}\left(1-\frac{r^2}{R^2}\right),\ 0 \le r \le R\ , \tag{53}$$

where the inner tube wall thickness is *R* and the distance of the thermocouple from the adiabatic face is *r*. Given the test conditions, it is anticipated that this correction will be ≈2 °C for an overall temperature difference between the surface and the gas of 30 °C. The uncertainty interval for the wall thermocouple is

$$\left(\delta T_w\right)^2 = \left(\frac{\partial T_w}{\partial T_t}\delta T_t\right)^2 + \left(\frac{\partial T_w}{\partial q'''}\delta q'''\right)^2 + \left(\frac{\partial T_w}{\partial R}\delta R\right)^2 + \left(\frac{\partial T_w}{\partial k_s}\delta k_s\right)^2 + \left(\frac{\partial T_w}{\partial r}\delta r\right)^2\ . \tag{54}$$

The partial derivatives for each term are as follows:

$$\frac{\partial T_w}{\partial T_t} = 1\ , \tag{55}$$

$$\frac{\partial T_w}{\partial q'''} = -\frac{R^2}{2k_s}\left(1-\frac{r^2}{R^2}\right) = -\frac{\left(0.084(0.0254)\right)^2}{2(17)}\left(1-\frac{0.049^2}{0.084^2}\right)\ , \tag{56}$$

$$\frac{\partial T_w}{\partial R} = -\frac{q'''R}{k_s} = -\frac{(4)888\left(0.084(0.0254)\right)}{\pi\left(0.625^2-0.457^2\right)18(0.0254)^3 17}\ , \tag{57}$$

$$\frac{\partial T_w}{\partial k_s} = \frac{q'''R^2}{2k_s^2}\left(1-\frac{r^2}{R^2}\right) = \frac{(4)888\left(0.084(0.0254)\right)^2}{\pi\left(0.625^2-0.457^2\right)18(0.0254)^3 2(17)^2}\left(1-\frac{0.049^2}{0.084^2}\right)\ , \tag{58}$$

and

$$\frac{\partial T_w}{\partial r} = \frac{q'''r}{k_s} = \frac{(4)888\left(0.049(0.0254)\right)}{\pi\left(0.625^2-0.457^2\right)18(0.0254)^3 17}\ . \tag{59}$$

The uncertainty interval for the thermocouple measurement is

$$\left(\delta T_t\right)^2 = \left(\delta T_{\text{Wire}}\right)^2 + \left(\delta T_{\text{IcePoint}}\right)^2 + \left(\delta T_{\text{Round}}\right)^2 + \left(\delta T_{\text{Attach}}\right)^2\ , \tag{60}$$

$$\left(\delta T_t\right)^2 = \left(1.10\right)^2 + \left(0.05\right)^2 + \left(0.01\right)^2 + \left(0.10\right)^2\ , \tag{61}$$

and

$$T_t = 321.4 \pm 1.11 \text{ K (20 to 1).} \tag{62}$$

The uncertainty intervals for the tube wall thickness, R, and radial position or the thermocouple, r, are taken from fabrication drawings:

$$(\delta R)^2 = (0.015/2)^2 + (0.005/2)^2 \text{ and } (\delta r)^2 = (0.015/2)^2 \ . \tag{63}$$

The uncertainty interval for thermal conductivity of the solid tube wall is assumed negligible.

C.3.6 Gas Temperature Uncertainty Interval

For a constant surface heat flux condition, mean gas temperature as it flows through a channel is a linear function of position, $T_g(x) = T_i + \frac{q\pi d_o}{mc_g} x$. If the outlet temperature and channel length are known, the relation between temperature and position can be simplified to

$$T_g(x) = T_i + (T_o - T_i)\frac{x}{L} \ , \tag{64}$$

where $0 \le x \le L$.

The uncertainty interval is then

$$\delta T^2 = \left(\left(1 - \frac{x}{L}\right)\delta T_i\right)^2 + \left(\left(\frac{x}{L}\right)\delta T_o\right)^2 + \left(\left(\frac{T_o - T_i}{L}\right)\delta x\right)^2 \ . \tag{65}$$

Substituting values into this equation yields

$$\delta T^2 = \left(\left(1 - \frac{9}{18}\right)1.1\right)^2 + \left(\left(\frac{9}{18}\right)1.1\right)^2 + \left(\left(\frac{311 - 271}{18}\right)0.1\right)^2 \tag{66}$$

$$T_g = 291.1 \pm 1.12 \text{ K (20 to 1).} \tag{67}$$

C.3.7 Gas Thermal Conductivity Uncertainty Interval

Values for the thermal conductivity of gas mixtures have not been firmly established over a wide temperature range by either theory or test. At low pressure, gas thermal conductivity is a function of its composition and temperature. Deviations between measured and theoretical values can often range ±10%. For this estimate, the functional relation described in appendix A will be assumed to correspond to the data and an uncertainty interval will be established based on uncertainties in temperature and composition using numerically calculated partial derivatives:

$$\delta k_g^2 = \left(\frac{\partial k_g^2}{\partial T_g} \delta T_g \right)^2 + \left(\frac{\partial k_g^2}{\partial n} \delta n \right)^2 , \tag{68}$$

$$\delta k_g^2 = \left(\frac{(0.0648 - 0.0584)}{(311 - 271)} 1.1 \right)^2 + \left(\frac{(0.0754 - 0.0505)}{(0.3 - 0.5)} 0.02 \right)^2 , \tag{69}$$

and

$$k_g = 0.06170 \pm 0.00249 \text{ W/m-K (20 to 1)} . \tag{70}$$

C.3.8 Annulus Eccentricity Uncertainty

Annulus eccentricity is the distance between the centerlines of the inner and jacket tubes divided by the mean gap between the tubes. Eccentricity can affect local Nusselt numbers as shown in Rohsenow, Hartnett, and Ganic.[8] A linear relation is adopted between Nusselt number and eccentricity. Eccentricity is estimated based on measurements of total indicated runout of the inner and jacket tubes which are 0.0085 in and 0.005 in, respectively:

$$e = \frac{2e^*}{D_i - d_o} = \frac{2\left((tir_i)^2 + (tir_o)^2 \right)^{1/2}}{D_i - d_o} = \frac{2\left((0.0085)^2 + (0.005)^2 \right)^{1/2}}{0.815 - 0.625} \tag{71}$$

$$e = 0 \pm 0.104 \text{ (20 to 1)} . \tag{72}$$

C.3.9 Reynolds Number Uncertainty

The Reynolds number for a fluid flowing through a circular annulus, $Re = 4q\,[c_g(T_o - T_i)\,\pi(D_i + d_o)\mu]^{-1}$, can be described as a function of heating rate, temperature rise across the test section, the principle diameters of the passage, gas specific heat, and viscosity. It is used here as an independent variable in correlation of the nondimensional friction factor and the heat transfer rate.

Uncertainty in experimental variables and results at $r^* = 0.833$, $r^* = 0.878$, $r^* = 0.714$, and $r^* = 0.500$ are shown in tables 9–12, respectively.

Table 9. Uncertainty in experimental variables and results at $r^* = 0.833$.

Variable	Value ± Uncertainty	Description	Interval
Gas	He-40Ar ± 2%	Gas composition	0.02
E	$2.0518 \pm 6.16 \times 10^{-4}$ V	Terminal voltage	0.0003
I	413 ± 0.54 A	Current through test section	0.0013
R	$4.97 \times 10^{-3} \pm 6.63 \times 10^{-6}$ ohm	Resistance of test section	0.0013
q	848 ± 3.78 W	Power supplied to inner tube	0.0045
q_o	–3.61 ± 0.63 W	Heat loss (insulation only)	0.1751
q'''	$2.01 \times 10^{7} \pm 6.86 \times 10^{5}$ W/m^3	Volumetric heating rate	0.0341
T_t	330.27 ± 1.1 K	Embedded thermocouple temperature	0.0293
T_w	328.49 ± 1.61 K	Surface temperature at tube OD	0.043
T_o	311 ± 1.1 K	Outlet temperature from test section	0.0293
T_a	300 ± 1.1 K	Room temperature	0.0293
T_g	291 ± 1.12 K	Bulk gas temperature	0.0299
T_i	271 ± 1.1 K	Inlet temperature to test section	0.0293
T_w-T_g	37.49 ± 1.96 K	Wall to gas temperature difference	0.0523
T_t-T_w	1.78 ± 1.18 K	Thermocouple to surface drop	0.6615
L_t	25 ± 0.01 K	Test section total length	0.0004
L_a	18 ± 0.01 K	Test section active length	0.0006
x	9 ± 0.1 in	Measurement position	0.0111
D_s	6 ± 0.1 in	Insulation outside diameter	0.0167
D_o	1.25 ± 0.005 in	Jacket outside diameter	0.004
D_i	0.75 ± 0.002 in	Jacket inside diameter	0.0027
D_i	0.75 ± 0.005 in	Jacket total indicated runout	0.0067
d_o	0.625 ± 0.005 in	Inner tube outside diameter	0.008
d_o	0.625 ± 0.009 in	Inner tube total indicated runout	0.0136
d	0.555 ± 0.005 in	Thermocouple diameteral location	0.009
d_i	0.457 ± 0.015 in	Inner tube inside diameter	0.0328
d_h	0.125 ± 0.004 in	Hydraulic diameter	0.0282
R	0.084 ± 0.016 in	Inner tube wall thickness	0.1882
r	0.049 ± 0.016 in	Thermocouple to adiabatic face distance	0.3227
A	35.33 ± 0.344 in^2	Heat transfer area	0.0097
k_g	$0.066 \pm 2.5 \times 10^{-3}$ W/m-K	Gas thermal conductivity	0.0379
c_g	$1{,}131 \pm 1.13 \times 10^{1}$ J/kg-K	Gas specific heat	0.01
μ_g	$2.28 \times 10^{-5} \pm 2.85 \times 10^{-7}$ kg/m-s	Gas viscosity	0.0125
c_s	$400 \pm 4 \times 10$ J/kg-K	Stainless steel heat capacity	0.01
k_s	$17 \pm 1.7 \times 10^{-1}$ W/m-K	Stainless steel thermal conductivity	0.01
ρ_s	$7{,}900 \pm 7.9 \times 10^{1}$ kg/m^3	Stainless steel density	0.01
r_s	$7.2 \times 10^{-7} \pm 7.2 \times 10^{-9}$ ohm-m	Stainless steel resistivity	0.01
k_i	$0.068 \pm 6.8 \times 10^{-4}$ W/m-K	Insulation conductivity vermiculite	0.01
e	0 ± 0.158	Eccentricity	0.0789
Re	30,000 ± 1,294	Reynolds number	0.0431
Pr	0.39 ± 0.02	Prandtl number	0.0404
Nu	47.8 ± 91.1	Nusselt number	1.9059

Table 10. Uncertainty in experimental variables and results at $r^* = 0.767$.

Variable	Value ± Uncertainty	Description	Interval
Gas	He-40Ar ± 2%	Gas composition	0.02
E	$1.7817 \pm 5.35\times10^{-4}$ V	Terminal voltage	0
I	498 ± 0.65 A	Current through test section	0.001
R	$3.58\times10^{-3} \pm 4.77\times10^{-6}$ ohm	Resistance of test section	0.001
q	888 ± 3.91 W	Power supplied to inner tube	0.004
q_o	–3.73 ± 0.65 W	Heat loss (insulation only)	0.175
q'''	$2.11\times10^{7} \pm 7.19\times10^{5}$ W/m^3	Volumetric heating rate	0.034
T_t	352.54 ± 1.1 K	Embedded thermocouple temperature	0.018
T_w	350.68 ± 1.65 K	Surface temperature at tube OD	0.028
T_o	311 ± 1.1 K	Outlet temperature from test section	0.018
T_a	300 ± 1.1 K	Room temperature	0.018
T_g	291 ± 1.12 K	Bulk gas temperature	0.019
T_i	271 ± 1.1 K	Inlet temperature to test section	0.018
T_w-T_g	59.68 ± 2 K	Wall to gas temperature difference	0.033
T_t-T_w	1.86 ± 1.23 K	Thermocouple to surface drop	0.662
L_t	25 ± 0.01 K	Test section total length	0
L_a	18 ± 0.01 K	Test section active length	0.001
x	9 ± 0.1 in	Measurement position	0.011
D_s	6 ± 0.1 in	Insulation outside diameter	0.017
D_o	1.315 ± 0.005 in	Jacket outside diameter	0.004
D_i	0.815 ± 0.002 in	Jacket inside diameter	0.002
D_i	0.815 ± 0.005 in	Jacket total indicated runout	0.006
d_o	0.625 ± 0.005 in	Inner tube outside diameter	0.008
d_o	0.625 ± 0.009 in	Inner tube total indicated runout	0.014
d	0.555 ± 0.005 in	Thermocouple diameteral location	0.009
d_i	0.457 ± 0.015 in	Inner tube inside diameter	0.033
d_h	0.19 ± 0.004 in	Hydraulic diameter	0.019
R	0.084 ± 0.016 in	Inner tube wall thickness	0.188
r	0.049 ± 0.016 in	Thermocouple to adiabatic face distance	0.323
A	35.33 ± 0.344 in^2	Heat transfer area	0.010
k_g	$0.066 \pm 2.5\times10^{-3}$ W/m-K	Gas thermal conductivity	0.038
c_g	$1{,}131 \pm 1.13\times10^{1}$ J/kg-K	Gas specific heat	0.01
μ_g	$2.28\times10^{-5} \pm 2.85\times10^{-7}$ kg/m-s	Gas viscosity	0.013
c_s	$400 \pm 4\times10$ J/kg-K	Stainless steel heat capacity	0.01
k_s	$17 \pm 1.7\times10^{-1}$ W/m-K	Stainless steel thermal conductivity	0.01
ρ_s	$7{,}900 \pm 7.9\times10^{1}$ kg/m^3	Stainless steel density	0.01
r_s	$7.2\times10^{-7} \pm 7.2\times10^{-9}$ ohm-m	Stainless steel resistivity	0.01
k_i	$0.068 \pm 6.8\times10^{-4}$ W/m-K	Insulation conductivity vermiculite	0.01
e	0 ± 0.104	Eccentricity	0.052
Re	30,000 ± 1,293	Reynolds number	0.043
Pr	0.39 ± 0.0166	Prandtl number	0.042
Nu	47.8 ± 4.11	Nusselt number	0.086

Table 11. Uncertainty in experimental variables and results at $r^* = 0.714$.

Variable	Value ± Uncertainty	Description	Interval
Gas	He-40Ar ± 2%	Gas composition	0.02
E	$1.8184 \pm 5.46 \times 10^{-4}$ V	Terminal voltage	0
I	509 ± 0.66 A	Current through test section	0.001
R	$3.58 \times 10^{-3} \pm 4.77 \times 10^{-6}$ ohm	Resistance of test section	0.001
q	925 ± 4.04 W	Power supplied to inner tube	0.004
q_o	–3.84 ± 0.67 W	Heat loss (insulation only)	0.175
q'''	$2.2 \times 10^{7} \pm 7.49 \times 10^{5}$ W/m^3	Volumetric heating rate	0.034
T_t	374.74 ± 1.1 K	Embedded thermocouple temperature	0.013
T_w	372.8 ± 1.69 K	Surface temperature at tube OD	0.021
T_o	311 ± 1.1 K	Outlet temperature from test section	0.013
T_a	300 ± 1.1 K	Room temperature	0.013
T_g	291 ± 1.12 K	Bulk gas temperature	0.014
T_i	271 ± 1.1 K	Inlet temperature to test section	0.013
T_w-T_g	81.8 ± 2.03 K	Wall to gas temperature difference	0.025
T_t-T_w	1.94 ± 1.28 K	Thermocouple to surface drop	0.662
L_t	25 ± 0.01 K	Test section total length	0
L_a	18 ± 0.01 K	Test section active length	0.001
x	9 ± 0.1 in	Measurement position	0.011
D_s	6 ± 0.1 in	Insulation outside diameter	0.017
D_o	1.375 ± 0.005 in	Jacket outside diameter	0.004
D_i	0.875 ± 0.002 in	Jacket inside diameter	0.002
D_i	0.875 ± 0.005 in	Jacket total indicated runout	0.006
d_o	0.625 ± 0.005 in	Inner tube outside diameter	0.008
d_o	0.625 ± 0.009 in	Inner tube total indicated runout	0.014
d	0.555 ± 0.005 in	Thermocouple diameteral location	0.009
d_i	0.457 ± 0.015 in	Inner tube inside diameter	0.033
d_h	0.25 ± 0.004 in	Hydraulic diameter	0.014
R	0.084 ± 0.016 in	Inner tube wall thickness	0.188
r	0.049 ± 0.016 in	Thermocouple to adiabatic face distance	0.323
A	35.33 ± 0.344 in^2	Heat transfer area	0.01
k_g	$0.066 \pm 2.5 \times 10^{-3}$ W/m-K	Gas thermal conductivity	0.038
c_g	$1{,}131 \pm 1.13 \times 10^{1}$ J/kg-K	Gas specific heat	0.01
μ_g	$2.28 \times 10^{-5} \pm 2.85 \times 10^{-7}$ kg/m-s	Gas viscosity	0.013
c_s	$400 \pm 4 \times 10$ J/kg-K	Stainless steel heat capacity	0.01
k_s	$17 \pm 1.7 \times 10^{-1}$ W/m-K	Stainless steel thermal conductivity	0.01
ρ_s	$7{,}900 \pm 7.9 \times 10^{1}$ kg/m^3	Stainless steel density	0.01
r_s	$7.2 \times 10^{-7} \pm 7.2 \times 10^{-9}$ ohm-m	Stainless steel resistivity	0.01
k_i	$0.068 \pm 6.8 \times 10^{-4}$ W/m-K	Insulation conductivity vermiculite	0.01
e	0 ± 0.079	Eccentricity	0.039
Re	30,000 ± 1,293	Reynolds number	0.043
Pr	0.39 ± 0.02	Prandtl number	0.04
Nu	47.8 ± 2.99	Nusselt number	0.063

Table 12. Uncertainty in experimental variables and results at $r^* = 0.500$.

Variable	Value ± Uncertainty	Description	Interval
Gas	He-40Ar ± 2%	Gas composition	0.02
E	$2.0331 \pm 6.1 \times 10^{-4}$ V	Terminal voltage	0
I	569 ± 0.74 A	Current through test section	0.001
R	$3.58 \times 10^{-3} \pm 4.77 \times 10^{-6}$ ohm	Resistance of test section	0.001
q	1,156 ± 4.85 W	Power supplied to inner tube	0.004
q_o	–4.6 ± 0.81 W	Heat loss (insulation only)	0.175
q'''	$2.75 \times 10^{7} \pm 9.35 \times 10^{5}$ W/m^3	Volumetric heating rate	0.034
T_t	549.04 ± 1.1 K	Embedded thermocouple temperature	0.004
T_w	546.62 ± 1.95 K	Surface temperature at tube OD	0.008
T_o	311 ± 1.1 K	Outlet temperature from test section	0.004
T_a	300 ± 1.1 K	Room temperature	0.004
T_g	291 ± 1.12 K	Bulk gas temperature	0.004
T_i	271 ± 1.1 K	Inlet temperature to test section	0.004
T_w-T_g	255.62 ± 2.24 K	Wall to gas temperature difference	0.009
T_t-T_w	2.43 ± 1.6 K	Thermocouple to surface drop	0.662
L_t	25 ± 0.01 K	Test section total length	0
L_a	18 ± 0.01 K	Test section active length	0.001
x	9 ± 0.1 in	Measurement position	0.011
D_s	6 ± 0.1 in	Insulation outside diameter	0.017
D_o	1.75 ± 0.005 in	Jacket outside diameter	0.003
D_i	1.25 ± 0.002 in	Jacket inside diameter	0.002
D_i	1.25 ± 0.005 in	Jacket total indicated runout	0.004
d_o	0.625 ± 0.005 in	Inner tube outside diameter	0.008
d_o	0.625 ± 0.009 in	Inner tube total indicated runout	0.014
d	0.555 ± 0.005 in	Thermocouple diameteral location	0.009
d_i	0.457 ± 0.015 in	Inner tube inside diameter	0.033
d_h	0.625 ± 0.004 in	Hydraulic diameter	0.006
R	0.084 ± 0.016 in	Inner tube wall thickness	0.188
r	0.049 ± 0.016 in	Thermocouple to adiabatic face distance	0.323
A	35.33 ± 0.344 in^2	Heat transfer area	0.01
k_g	$0.066 \pm 2.5 \times 10^{-3}$ W/m-K	Gas thermal conductivity	0.038
c_g	$1{,}131 \pm 1.13 \times 10^{1}$ J/kg-K	Gas specific heat	0.01
μ_g	$2.28 \times 10^{-5} \pm 2.85 \times 10^{-7}$ kg/m-s	Gas viscosity	0.013
c_s	$400 \pm 4 \times 10$ J/kg-K	Stainless steel heat capacity	0.01
k_s	$17 \pm 1.7 \times 10^{-1}$ W/m-K	Stainless steel thermal conductivity	0.01
ρ_s	$7{,}900 \pm 7.9 \times 10^{1}$ kg/m^3	Stainless steel density	0.01
r_s	$7.2 \times 10^{-7} \pm 7.2 \times 10^{-9}$ ohm-m	Stainless steel resistivity	0.01
k_i	$0.068 \pm 6.8 \times 10^{-4}$ W/m-K	Insulation conductivity vermiculite	0.01
e	0 ± 0.032	Eccentricity	0.016
Re	30,000 ± 1,294	Reynolds number	0.043
Pr	0.39 ± 0.02	Prandtl number	0.04
Nu	47.8 ± 2.09	Nusselt number	0.044

REFERENCES

1. Glassman, A.J.: "Summary of Brayton Cycle Analytical Studies for Space Power System Applications," *NASA TN D-2487*, Glenn Research Center, Cleveland, OH, 1964.

2. Bragg-Sitton, S.M.; Kapernick, R.; and Godfroy, T.J.: "Single Channel Testing for Characterization of the Direct Gas Cooled Reactor and the SAFE-100 Heat Exchanger," in *Proceedings Space Technology and Applications International Forum (STAIF-2004)*, Albuquerque, NM, Vol. 699, pp. 741–748, February 2004.

3. Touloukian, Y.S.; Liley, P.E.; and Saxena, S.C.: *Thermophysical Properties of Matter, Volume 3, Thermal Conductivity*, IFI/Plenum, New York, 1981a.

4. Touloukian, Y.S.; Saxena, S.C.; and Hestermans, P.: *Thermophysical Properties of Matter, Volume 11, Viscosity*, IFI/Plenum, New York, 1981b.

5. Hirschfelder, J.O.; Curtiss, C.F.; and Bird, R.B.: *Molecular Theory of Gases and Liquids*, Wiley, New York, 1964.

6. Vanco, M.R.: "Analytical Comparison of Relative Heat Transfer Coefficients and Pressure Drops of Inert Gases and Their Binary Mixtures," *NASA TN D-2677*, 1965.

7. Walker, J.E.; Whan, G.A.; and Rothfus, R.R.: "Fluid Friction in Noncircular Ducts," *AIChE J.*, Vol. 3, pp. 484–489, December 1957.

8. Rohsenow, W.M.; Hartnett, J.P.; and Ganic, E.N.: *Handbook of Heat Transfer Fundamentals,* 2nd ed., McGraw-Hill, New York, 1985.

9. Taylor, M.F.; Bauer, K.E.; and McEligot, D.M.: "Internal Forced Convection to Low-Prandtl Number Gas Mixtures," *Int. J. Heat Mass Transfer*, Vol. 31, pp. 13–25, 1988.

10. Kays, W.M.; and Leung, E.Y.: "Heat Transfer in Annular Passages—Hydrodynamically Developed Turbulent Flow With Arbitrarily Prescribed Heat Flux," *Int. J. Heat Mass Transfer*, Vol. 6, pp. 537–557, 1963.

11. Wilson, N.W.; and Medwell, J.O.: "An Analysis of Heat Transfer for Fully Developed Turbulent Flow in Concentric Annuli," *J. Heat Transfer*, Vol. 90(1), p. 43, 1968.

12. Taylor, M.F.; Bauer, K.E.; and McEligot, D.M.: "Internal Forced Convection to Low-Prandtl-Number Gas Mixtures," *Int. J. Heat Mass Transfer*, Vol. 31(1), pp. 13–25, 1988.

13. McEligot, D.M.; and Taylor, M.F.: "The Turbulent Prandtl Number in the Near-Wall Region for Low-Prandtl Number Gas Mixtures," *Int. J. Heat Mass Transfer*, Vol. 39, pp. 1287–1295, 1996.

14. Kays, W.M.: *Convective Heat and Mass Transfer*, 1st ed., McGraw-Hill, New York, 1966.

15. Kays, W.M.; Crawford, M.E.; and Weigand, B.: *Convective Heat and Mass Transfer*, 4th ed., McGraw-Hill, New York, 2005.

16. Petukhov, B.S.: "Heat Transfer and Friction in Turbulent Pipe Flow With Variable Physical Properties," *Advances in Heat Transfer*, J.P. Hartnett and T.F. Irvine, eds., Academic Press, New York, 1970.

17. Colburn, A.P.: "A Method of Correlating Forced Convection Heat Transfer Data and a Comparison With Fluid Friction," *Trans. AIChE*, Vol. 29, p. 174, 1933.

18. Dittus, F.W.; and Boelter, L.M.K.: University of California, Berkeley Publications on Engineering, Vol. 2, p. 443, 1930.

19. Maubach, K.: "Rough Annulus Pressure Drop—Interpretation of Experiments and Recalculation for Square Ribs," *Int. J. Heat Mass Transfer*, Vol. 15, pp. 2489–2498, 1972.

20. Dalle-Donne, M.; and Merrwalds, E.: "Heat Transfer and Friction Coefficients For Turbulent Flow of Air In Smooth Annuli at High Temperatures," *Int. J. Heat Mass Transfer*, Vol. 16, pp. 781–809, 1973.

21. Ichimiya, K.: "Effects of Several Roughness Elements on an Insulated Wall for Heat Transfer Form the Opposite Smooth Heated Surface in a Parallel Plate Duct," *J. Heat Transfer*, Vol. 109, pp. 68–73, 1987.

22. Takase, K.: "Experimental and Analytical Studies on Turbulent Heat Transfer Performance of a Fuel Rod With Spacer Ribs for High Temperature Gas-cooled Reactors," *Nuclear Engineering and Design*, Vol. 154, pp. 345–356, 1995.

23. Jonsson, V.K.; and Sparrow, E.M.: "Turbulent Diffusivity for Momentum Transfer in Concentric Annuli," *J. Basic Eng.*, Vol. 88, pp. 550–552, 1966.

24. Kays, W.M.: *Compact Heat Exchangers*, McGraw-Hill Co., New York, 1964.

25. Holman, J.P.: *Heat Transfer*, 5th ed., McGraw-Hill, New York, pp. 121–127, 1981.

26. Jain, P.C.: "The Prediction of the Thermal Conductivity of Xenon," *J. Phys. D*: *Appl. Phys.*, Vol. 11, pp. 2371–2373, 1978.

27. Jody, B.J.; Saxena, S.C.; Nain, V.P.S.; and Aziz, R.A.: 1976 *High Temp. Sci.,* Academic Press, New York, Vol. 8, p. 343, 1976.

28. Ho, C.Y.; Powell, R.W.; and Liley, P.E.: “Thermal Conductivity of the Elements: A Comprehensive Review,” *J. Phys. Chem. Ref. Data*, Supplement 1, Vol. 3, pp. 1–797, 1974.

29. Kline, S.J.; and McClintock, F.A.: “Describing Uncertainties in Single-Sample Experiments,” *Mech. Eng.,* Vol. 73(1), p. 38, 1953.

REPORT DOCUMENTATION PAGE

Form Approved
OMB No. 0704-0188

1. AGENCY USE ONLY *(Leave Blank)*	2. REPORT DATE	3. REPORT TYPE AND DATES COVERED
	November 2007	Technical Memorandum

4. TITLE AND SUBTITLE

Heat Transfer and Pressure Drop in Concentric Annular Flows of Binary Inert Gas Mixtures

5. FUNDING NUMBERS

6. AUTHORS

R.S. Reid, J.J. Martin, D.J. Yocum,* and E.T. Stewart

7. PERFORMING ORGANIZATION NAME(S) AND ADDRESS(ES)

George C. Marshall Space Flight Center
Marshall Space Flight Center, AL 35812

8. PERFORMING ORGANIZATION REPORT NUMBER

M–1210

9. SPONSORING/MONITORING AGENCY NAME(S) AND ADDRESS(ES)

National Aeronautics and Space Administration
Washington, DC 20546–0001

10. SPONSORING/MONITORING AGENCY REPORT NUMBER

NASA/TM—2007–215135

11. SUPPLEMENTARY NOTES

Prepared by the Propulsion Systems Department, Engineering Directorate *Graduate Student Research Program employee in support of Marshall Space Flight Center.

12a. DISTRIBUTION/AVAILABILITY STATEMENT

Unclassified-Unlimited
Subject Category 34
Availability: NASA CASI 301–621–0390

12b. DISTRIBUTION CODE

13. ABSTRACT *(Maximum 200 words)*

Studies of heat transfer and pressure drop of binary inert gas mixtures flowing through smooth concentric circular annuli, tubes with fully developed velocity profiles, and constant heating rate are described. There is a general lack of agreement among the constant property heat transfer correlations for such mixtures. No inert gas mixture data exist for annular channels. The intent of this study was to develop highly accurate and benchmarked pressure drop and heat transfer correlations that can be used to size heat exchangers and cores for direct gas Brayton nuclear power plants. The inside surface of the annular channel is heated while the outer surface of the channel is insulated. Annulus ratios range $0.5 < r^* < 0.83$. These smooth tube data may serve as a reference to the heat transfer and pressure drop performance in annuli, tubes, and channels having helixes or spacer ribs, or other surfaces.

14. SUBJECT TERMS

heat transfer, low Prandtl number, thermal hydraulics, gas mixtures

15. NUMBER OF PAGES

80

16. PRICE CODE

17. SECURITY CLASSIFICATION OF REPORT	18. SECURITY CLASSIFICATION OF THIS PAGE	19. SECURITY CLASSIFICATION OF ABSTRACT	20. LIMITATION OF ABSTRACT
Unclassified	Unclassified	Unclassified	Unlimited

National Aeronautics and
Space Administration
IS20
George C. Marshall Space Flight Center
Marshall Space Flight Center, Alabama
35812